A Prospective Cohort Study to Estimate the Effect of Ultrafine Particulate Matter (UFP) Air Pollution on Alzheimer's Disease Neuropathology at Autopsy in Puget Sound and A Case Study to Establish Research Methodology to apply AERMOD to model SEATAC Airport Aircraft Traffic Flow UFP Emission

Kwokyan Tsoi

A thesis

submitted in partial fulfillment of the

requirements for the degree of

Master of Public Health (Occupational and Environmental Medicine)

University of Washington

2023

Committee:

Lianne Sheppard

Elena Austin

Debra Cherry

Timothy Larson

Program Authorized to Offer Degree:

Environmental and Occupational Health Sciences

University of Washington

Abstract

A Prospective Cohort Study to Estimate the Effect of Ultrafine Particulate Matter (UFP) Air Pollution on Alzheimer's Disease Neuropathology at Autopsy in Puget Sound and A Case Study to Establish Research Methodology to apply AERMOD to model SEATAC Airport Aircraft Traffic Flow UFP Emission

Kwokyan Tsoi

Chair of the Supervisory Committee:

Lianne Sheppard

Department of Environmental and Occupational Health Science

Introduction: This project has two sections, the first addressing the association between ultrafine particle (UFP) air pollution exposure and neuropathology outcomes, and the second a case study to better characterize airplane exhaust emission distribution to ultimately characterize UFP exposures.

Section One: A Prospective Cohort Study to Estimate the Effect of Ultrafine Particulate Matter (UFP) Air Pollution on Alzheimer's Disease Neuropathology at Autopsy in Puget Sound

Background: Evidence links air pollution to Alzheimer’s disease (AD). The health effects of ultrafine particulate matter (UFP) air pollution are not well understood, and no community-based

prospective cohort studies in older adults have evaluated the association between UFP and markers of AD neuropathology at autopsy.

Objective: Using a well-established autopsy cohort from the Adult Changes in Thought (ACT) study and UFP predictions from a mobile monitoring campaign, we evaluated the associations of 10-year annual average UFP exposure prior to death with Braak staging and Consortium to Establish a Registry for AD (CERAD) scores.

Methods: We used autopsy specimens (N=608) from the ACT study, with year of death 2005 and after. We assigned annual average UFP exposure at residential address based on ACT UFP exposure spatial model. We dichotomized the outcome variables with a cutoff of Braak staging V and VI, and CERAD scores moderate and frequent. Adjusting for confounders and precision variables in the analysis, we performed logistic regression on the dichotomous outcomes.

Results: The average 10-year average UFP exposure from death across the 608 autopsy samples was 10292 particles per cm^3 (pt/cm^3), while interquartile range (IQR) was 1913 pt/cm^3. For every IQR increase in 10-year average UFP, the odds of having a significant Braak stage was estimated to be 0.95 with a 95% confidence interval ranging between 0.80 and 1.11; the odds of having a significant CERAD score was estimated to be 0.97 with a 95% confidence interval ranging between 0.82 and 1.13; the odds of having both significant Braak stage and CERAD scores was estimated to be 0.94 with a 95% confidence interval ranging between 0.79 and 1.11.

Conclusion: Our result is consistent with a wide range of effects including both increased risk and protective effects of UFP exposure on AD neuropathology. We have enough evidence to know UFP is not highly protective against AD neuropathology. It is possible the level of UFP in Puget Sound has no health effects. Our study methodology has implication in assessing UFP health impact in other cities.

Section Two: A Case Study to Establish Research Methodology to apply AERMOD to model SEATAC Airport Aircraft

Background: Aircrafts are high-level UFP producers. Aircraft traffic flows for international airports, including SEATAC airport serving the Seattle metropolitan area, are very high. The current ACT spatial model detects an elevation of UFP near SEATAC airport. The ACT spatial model does not distinguish between exposures among different sources.

Objective: Using National Oceanic and Atmospheric Association (NOAA) meteorological data, Federal Aviation Association (FAA) flight traffic data, National Elevation Database (NED), we characterize SEATAC 2019 annual average aircraft traffic flow UFP emission distribution using AERMOD modeling.

Methods: We separate the SEATAC aircraft traffic flow into four independent simulations based on traffic direction and purpose: south flow landing, south flow takeoff, north flow landing, north flow takeoff. The emission of flight paths which the aircrafts descend from or ascend to 1000 meters are simulated by line volume sources. Ground detectors are simulated by a receptor grid 86 kilometers longitudinally and 40 kilometers latitudinally centered at runway 3 of SEATAC airport. 2019 FAA flight traffic data determines when the line volume sources emit. NOAA and NED data are utilized by AERMOD through AERMET and AERMAP.

Results:

AERMOD output predicts high aircraft traffic flow emission distribution north of SEATAC airport and south of downtown Seattle. Emission distributions have a sharp peak and reduction on both sides of the peak. Peak emissions are right under the flight paths. One kilometer away from the flight paths, the distributions reduce to 5% of maximum.

Conclusion:

Our AERMOD simulations suggest SEATAC aircraft traffic may lead to focally elevated UFP exposure for people living under the flight paths. Future research should incorporate these AERMOD predictions into a revised ACT spatial model. The implications of this work may extend far beyond this case study to improve UFP exposure predictions around airports in other areas.

TABLE OF CONTENTS

LIST OF TABLES

LIST OF FIGURES

THESIS INTRODUCTION:

My research goal is to investigate whether there is an association between ultrafine particulate matter (UFP) and Alzheimer's disease (AD). Evidence has linked air pollution with worsening progression of Alzheimer's disease [1]. UFP in air pollution is hypothesized to be impactful for brain health because of its small size. Animal toxicity studies observed UFP translocated into mice brains [12]. UFP health effects in humans are currently poorly understood [11-14]. AD is the most common form of dementia, and it is very expensive to treat and manage [1]. Understanding the UFP impact on AD can help guide new interventions that could prevent significant morbidity while lowering health care costs.

UFP sources include both aircraft traffic, road traffic, and industrial land use. Different sources can have different UFP distribution patterns [32].

My thesis has two aims. In aim 1, we use a prospective cohort study to evaluate the association between UFP exposure and AD neuropathology at autopsy using a well-established cohort in Puget Sound. Aim 1 tests the hypothesis of increased UFP exposure is associated with increased in significant AD neuropathology findings in autopsy. Aim 1 is discussed in Section 1 of my thesis. Aim 2 is a case study to establish the methodology to use AERMOD to simulate aircraft traffic flow UFP emission at SEATAC airport. Aim 2 improves our characterization of UFP exposure. Section 2 discusses aim 2.

SECTION ONE: A Prospective Cohort Study to Estimate the Effect of Ultrafine Particulate Matter (UFP) Air Pollution on Alzheimer's Disease Neuropathology at Autopsy in Puget Sound

INTRODUCTION:

The most common cause of dementia is Alzheimer's disease (AD) [1]. The neuropathology hallmark for AD is the accumulation of intraneuronal tau aggregations (neurofibrillary tangles (NFTs)) at predictable brain regions. Diagnoses for AD can be made by AD neuropathology at autopsy [3,4,5]. AD care costs nearly 1 trillion US dollars worldwide globally in 2020. The number of people living with dementia globally is expected to be 152 million by 2050 [1].

The elderly population is at high risk of developing AD [1]. People are at higher risk if they are exposed to air pollution, which is hypothesized to increase brain inflammation and reduce protective antioxidants [18-20,22,23]. In animal toxicity studies, particulate matter exposure is associated with brain neuroinflammation and early AD neuropathology [15-17]. Neuroinflammation and deposits of Aβ1–42 have been found among children and young adults living with high level of air pollution [11-17]. Because of emerging epidemiological and pathological evidences associating elevated level of air pollution with higher AD risk, the scientific community recommends reducing exposure to air pollution to prevent the onset of AD [2].

UFP is the smallest size particulate matter in air pollution with diameter less than 100 nanometers [6]. Among different types of particulate matter, UFP's effect on AD is the least known. UFP is hypothesized to have negative health effect on brains. UFP's may enter mice brains through the olfactory bulb and cross blood brain barrier [12].

Whether UFP causes brain damage is a subject of debate [6-10, 64]. UFP may be associated with increased microglial cells concentration, a neuroinflammation marker, in brain autopsy studies performed in child and young adults [6-10,12, 64]. Our study intends to add epidemiological evidence to find out whether there is an association between UFP and AD.

A recent paper from our group evaluated the association between fine particulate matter (PM 2.5) and AD neuropathology autopsy results among elderly people participating in the Adult Changes in Thought (ACT) study [21]. There is not yet a previous study on UFP and AD neuropathology among the elderly population. This study will be the first to explore the association between long-term UFP exposure and AD neuropathology at autopsy among participants in the ACT prospective community-based cohort study in Seattle, Washington, USA [24]. Urban and suburban elderly (>65 years) population made up this cohort. Our analysis of UFP complements our previously reported investigation between the neuropathology in AD and neurotoxic effect of PM2.5, using the same cohort. [21].

METHODS:

Study Design:

The ACT study is a prospective community-based cohort study in Seattle, WA, USA. The sample population is randomly sampled from a large health maintenance organization (HMO) (Group Health, now Kaiser Permanente of Washington) beginning in 1994 and continuing to the present time [21, 24]. During enrollment, participants are all certified as cognitively intact/ “not demented” by the Cognitive Abilities Screening Instrument (CASI) and have CASI scores higher than 85. We limit our sample population to participants who have a year of death of 2005 or after. We assume that UFP exposures may be stable across years between 1995 to 2019.

Exposure Assessment:

We collected UFP particle count using TSI NanoScan 3910. It has different bins for collecting different category of particle sizes, which allows us to count particles with size 100 nanometer diameter and below [32].

A Toyota Prius brought the NanoScan to the air sample collection sites. After arrival to the site, we performed stationary collection for 2 minutes. Samples were collected from March 2019 to March 2020. Collection time was between 4AM to 11PM. The collection schedule achieved a temporal design to collect air samples at different times of the day and at different seasons for each air sample collection site. We obtained numerous air samples per site. We report the median particle count for each site as our exposure measurement [32].

The mobile monitoring region in the greater Seattle area was selected to cover all the ACT cohort participants' residential addresses within a 1200 land kilometer square area. The monitoring region covers west King County and southwest Snohomish County. 309 air sample collection sites were selected to collect samples across the region to be specifically representative of the ACT cohort [32].

Residential addresses have been collected and updated by the HMO billing department and ACT study staff. Participants who lived outside of or moved away from the area covered by the spatial exposure prediction model are excluded from this study. If a participant changed residential location within the UFP exposure area, that participant's UFP exposure is a weighted annual average calculated by the duration among all the residential locations.

We developed a spatial model based on universal kriging with partial least squares. Each ACT participant UFP exposure is calculated based on their residential address history geocoded and linked to predictions from this spatial model [32].

We assumed that the 10-year average annual UFP exposure for ten years prior to death is the appropriate exposure metric. We chose the 10-year period because we hypothesize that a long-term exposure average is the most biologically appropriate averaging time. Furthermore, several previous studies showed larger effect estimates over this exposure time frame [21,63].

Outcome Assessment:

Sonnen's study documented the preservation and evaluation for ACT study brain autopsy neuropathologic measures [27]. Briefly, brain tissues were fixed in formalin and then dissected. Dissected brain slices were again fixed in formalin. Immunohistochemistry was performed to stain NFTs. The scoring of NFTs neuropathology was evaluated based on CERAD scores and Braak staging.

Braak staging is a location classification for NFTs. Among patients with AD, NFTs have predictable, progressive, and orderly buildup in different locations of their brains. There are 6 stages for Braak staging: BI, BII, BIII, BIV, BV and BVI [5]. Only BV and BVI are strongly associated with dementia. BI and BII can be found in normal individuals. BIII and BIV are found in pre-dementia people with symptoms that may be too mild to be clinically diagnosed. We dichotomized Braak staging into significant (BV and BVI) and non-significant in our analysis (BI, BII, BIII, and BIV). Dichotomization of Braak staging in this manner is widely practiced scientifically because clinical diagnosis can be completed by the identification of BV and BVI at autopsy [28-30].

Consortium to Establish a Registry for AD (CERAD) scores (none; sparse; moderate; frequent) are used to qualify neurofibrillary tangles (NFTs) density. There are 4 categories of CERAD scores: frequent, moderate, sparse, and rare. CERAD scores frequent and moderate are significant for dementia, while CERAD scores sparse and none are not significant for

dementia [28,29]. We dichotomized CERAD scores into significant (frequent and moderate) and non- significant (sparse and rare). Dichotomization of CERAD scores in this manner is widely practiced scientifically, as recommended by National Institute on Aging and Reagan Institute (NIA-RI) and pathologists (Figure 1) [28-30, 80].

Dementia is a syndrome, not a specific disease. There are many causes for dementia besides AD, including vascular cognitive impairment, dementia with Lewy body, and Parkinson Disease which are not part of our study. [5,28,29,30,31].

Analysis:

My statistical analysis uses autopsy complete cases. We performed logistic regression on dichotomized outcomes to evaluate 10-year average annual UFP association with AD neuropathology.

We use the interquartile range (IQR) of UFP of the sample population as the increment for reporting odds ratios as this is a more scientifically meaningful quantity of interest than reporting for a single UFP particle. The interquartile range of UFP is meaningful because it is related to the distribution of our sample.

We report three effect estimates: the odds ratio of having significant Braak staging, CERAD scores, and both Braak and CERAD at autopsy between two populations whose average UFP exposure 10 years prior to death differs by one IQR.

Using logistic regression, we adjust for the following confounders and precision variables in multiple staged models. Model 1, our minimally adjusted model, has sex, binary APOE genotype (1 or more ε4 allele versus no ε4 alleles), and age at death [21, 37-39]. Model 2, our *a priori* model, has all the terms included in model 1 plus year of death [21], educational degree [21,40,41], and neighborhood median household income [21,42]. Model 3, our extended model,

has all the terms included in model 2 plus race [21, 43-45], ever smoker [21, 46,47], and regular exercise [21, 48,49]. Model 4, our mediation extended model, has all the terms included in model 3 plus body mass index (BMI) [21, 51,52], diabetes [21, 53-56], hypertension [21,57-59], and cardiovascular disease [21,60-62].

All data analysis performed used R version 4.1.2 [82].

RESULTS:

Descriptive statistics result:

Characteristics of our sample population are summarized in Table 1. As of July 2022, the number of participants who enrolled on or after 2005 and were eligible to be included in the autopsy analysis was 4749. Of these, 2424 died by the year 2022, and 746 out of the 2424 deceased individuals consented to autopsy. We have 608 complete cases.

Table 3 has the summary of the missing covariates. There are 92 individuals who consented to autopsy but pathologists were unable to obtain Braak staging and CERAD scores. Potential reasons for unable to obtain Braak staging and CERAD scores include the brain tissues were too damaged to complete autopsy. There are 27 individuals without UFP exposure data, which can result from incomplete residential address record or living outside the exposure area. There are 24 individuals without APOE genotype.

The complete cases enroll at an older age when compared to the overall sample population. When reviewing Table 1, the complete cases distributions of median household income, level of education, smoking status, regular exercise status, BMI, history of diabetes, hypertension and cardiovascular disease, and ratio of biological sex are similar to the general cohort.

The range of 10-year prior to death annual average UFP exposure for the sample population is between 4614 and 20276 pt/cm^3 with a median of 10350 pt/cm^3 (Table 1, Figure 2). The interquartile range for the sample population is 1913 pt/cm^3. This narrow interquartile range demonstrates that most ACT participants have their UFP exposure level closer to the median versus the extremes. Figure 3 compares UFP exposure range and median between individuals with both Braak staging and CERAD scores being significant versus not significant. Figure 4 compares UFP exposure range and median between individuals with CERAD scores being significant versus not significant. Figure 5 compares UFP exposure range and median between individuals with Braak staging being significant versus not significant.

The proportion of autopsy samples with significant Braak staging is 58%. The proportion of autopsy samples with significant CERAD scores is 43%. The proportion of autopsy samples with both significant CERAD scores and Braak staging is 37% (Table 1). Table 4 summarizes the number of individuals with both, either, or no Braak staging and CERAD scores being significant. There are 223 individuals who have both significant Braak staging and CERAD scores. 232 individuals have neither Braak staging nor CERAD scores being significant. 121 individuals have CERAD scores significant but Braak staging not significant. 32 individuals have Braak staging significant but CERAD scores not significant.

Table 5 shows the number of people with and without both significant Braak staging and CERAD scores versus with and without clinical dementia diagnoses. Chi-square tests on the relationship between AD neuropathology and clinical dementia diagnoses are significant with p value less than 0.001.

Analytical statistics result:

For every IQR increase in annual average UFP over the 10 years prior to death, the odds ratio of having a significant Braak staging is 0.95 with confidence interval between 0.80 and 1.11. The odds ratio of having a significant CERAD scores is 0.97 with confidence interval between 0.82 and 1.13. The odds ratio of having both Braak staging and CERAD scores is 0.94 with confidence interval between 0.79 and 1.11 (Table 2). Our results imply that UFP exposure has a wide range of effects, including no effects in in its association with AD neuropathology. Our minimally adjusted model and extended models have similar effect estimates and overlapping confidence intervals compared to our primary a priori analysis, suggesting that there is no strong evidence for residual confounding.

DISCUSSION:

Our study is the first to evaluate the association between outdoor ambient UFP exposure and AD neuropathology autopsy results in a community-based prospective cohort study of older adults. Our effect estimates suggest UFP exposure is consistent with a wide range of effects on AD neuropathology. We do not have enough evidence to rule out no association; we can rule out UFPs being highly protective with an odds ratio for both significant Braak staging and CERAD scores lower than 0.79 for an IQR increase in UFP; likewise, we can rule out UFPs being associated with an odds ratio higher than 1.11 per IQR increase.

We used a complete case analysis without accounting for selection in the cohort due to missing covariates, death, or autopsy consent. I recommend that future researchers use more advanced statistical analysis approaches, such as bootstrapping (resampling with duplication), to minimize the effect of selection in this analysis.

A major strength of our work is that we use a spatial UFP model developed specifically for the ACT cohort. This spatial UFP model utilizes many short-term air samples measured at locations geographically representative of the ACT cohort and temporarily balanced throughout Puget Sound in the year 2019 to estimate the annual average. Thus, the quality of spatial UFP model training data is very high, relative to other datasets available for UFP exposures. Therefore, we expect the spatial model to give good quality predictions for 2019, which we then assume are valid back to 1995.

Our spatial model can produce UFP exposure predictions across a large geographically area with high accuracy because of our many sample sites. Our spatial model may benefit by higher resolution at locations that are immediately adjacent to highly polluting sources. According to our aim 2 computer simulation, aircraft exhaust sources can have high concentrations peaks with sharp reduction over short distances. In our aim 2, people living directly under the flight paths of SEATAC airport may experience ten times elevation in UFP exposure, compared to people living just one kilometer away from the flight paths. Our spatial model has the potential to be flexibly improved by adding new temporal and geographic data sets. This in turn may affect the estimated odds ratios reported in this chapter.

Our study results may suffer from reverse causality between UFP exposure and AD neuropathology. Fine particulate matter and air pollution in general have been determined to cause premature death, and UFP is higher where the overall air pollution is higher [57,58]. High levels of air pollution may have caused premature cardiovascular death and prevented highly exposed individuals to live long enough to develop the same significant neuropathologic markers as are observed for longer-living participants who were not exposed. If reverse causality is

present, then it follows that even if UFP causes brain damage, our study may see a smaller number of exposed brains with significant AD neuropathology.

Animal toxicity studies have hypothesized that UFP may negatively affect brain health. For example, 2-week exposures to UFP in mice induced neuroinflammation and early pre-dementia AD neuropathology, including plaques [64]. In vitro studies suggested that UFP exposure increases plaque formation in mice hippocampus [65], and traffic related UFP exposure may lead to oxidative stress in mice neurons [66].

Our study has not collected indoor air quality data and the use of air filters and air conditioning which can mitigate ambient-source exposures. Obtaining this information is currently cost prohibitive at the scale necessary to incorporate into this autopsy dataset.

CONCLUSION:

In summary, our result is consistent with a wide range of effects including both increased risk and protective effects of UFP exposure on AD neuropathology. We are unable to conclude that increased UFP is associated with increased amount of AD neuropathology. We have enough evidence to know UFP is not highly protective against AD neuropathology. It is possible the level of UFP in Puget Sound has no health effects. Our study methodology has implications in assessing UFP health impacts in other cities.

Table 1: Descriptive statistics of the general cohort and autopsy cohort. Continuous variables presented as mean (standard deviation (SD)); categorical variables presented as n (%).

	Enrolled population who are alive or have death year 2005 and after (n=4749)	Enrolled population with death year 2005 and later (n= 2424)	A priori main model (autopsy), complete cases (n= 608)
	Mean(SD)	Mean(SD)	Mean(SD)
Baseline Age (y)	73(69,77)	75(70,80)	76(71,80)
Age at Death (y)	90(86,94)	90(86,95)	90(86,95)
ACT Cohort	n (% of the cohort)	n (% of the cohort)	n (% of the cohort)
Original	1654(35%)	1359(56%)	323(53%)
Expansion	752(16%)	554(23%)	162(27%)
Replacement	2343(49%)	511(21%)	123(20%)
Birth Cohort			
c.1890–1910	284(5%)	247(10%)	62(10%)
1915	539(11%)	485(20%)	154(25%)
1920	828(17%)	699(29%)	175(29%)
1925	845(17%)	561(23%)	128(21%)
c.1930–1950	2289(48%)	582(18%)	89(15%)
≥1 APOE 4 allele	1033(22%)	582(18%)	175(29%)
Female	2818(59%)	1439(59%)	349(57%)
White	4211(89%)	2179(90%)	569(94%)
Census Tract Median Household Income			
<35,000	426(9%)	226(9%)	61(10%)
35,000–49,999	1396(31%)	768(32%)	191(31%)

50,000–74,999	2223(49%)	1165(48%)	293(48%)
>75,000	532(12%)	254(11%)	63(10%)
Degree			
None	288(6%)	219(9%)	40(7%)
GED/High School	1639(35%)	1095(45%)	251(41%)
Bachelors	1192(25%)	523(22%)	151(25%)
Masters	840(18%)	269(11%)	86(14%)
Doctorate	305(6%)	108(5%)	34(6%)
Other	483(10%)	208(9%)	46(8%)
Smoking Status			
Never	2408(51%)	1143(47%)	278(46%)
Past	2138(45%)	1144(47%)	297(49%)
Current	190(4%)	128(5%)	31(5%)
Regular Exercise	3520(74%)	1711(71%)	442(73%)
Body Mass Index (BMI)			
Underweight/Normal	1574(34%)	798(34%)	226(38%)
Overweight	1575(34%)	808(34%)	201(34%)
Obese	1471(32%)	748(32%)	164(28%)
Diabetes	441(10%)	270(11%)	60(10%)
Cardiovascular Disease	330(7%)	218(9%)	55(9%)
Hypertension	1934(41%)	992(41%)	236(39%)
Annual Avg UFP ($1pt/cm^3$) for the 10-y Prior to death			
lowest		4614	4616
Q1		9458	9556

Median Q2		10292	10350
Q3		11370	11360
highest		20276	19837
IQR		1913	1803
Braak stage			
Clinically Significant			353(58%)
Not significant			255(42%)
Missing			0(0%)
CERAD score			
Clinically Significant			264(43%)
Not significant			344(57%)
Missing			0(0%)
Both Braak stage and CERAD score			
Clinically Significant			223(37%)
Not significant			385(63%)

Table 2: Odds ratios with confidence intervals for AD neuropathology versus UFP exposure for an interquartile range increase in UFP for each model

Increase in one UFP IQR 1913 pt/cm^3	Braak Binary Category Odds Ratio	CERAD Binary Category Odds Ratio	Both Braak and CERAD Significant Odds Ratio
M1 minimally adjusted model	0.94 (0.81, 1.10)	0.94 (0.81, 1.10)	0.94 (0.81, 1.09)
M2 a priori model	0.95 (0.81, 1.11)	0.97 (0.82, 1.13)	0.94 (0.79, 1.11)
M3 extended lifestyle model	0.95 (0.81, 1.12)	0.97 (0.82, 1.14)	0.94 (0.79, 1.11)
M4 extended lifestyle model with health conditions	0.98 (0.83, 1.69)	0.95 (0.80, 1.13)	0.96 (0.80, 1.15)

Table 3: Missing data summary

Consent to autopsy	746
Complete cases	608
Type of covariate	Number of individuals missing that covariate
Braak staging	97
CERAD score	92
UFP exposure value	29
Sex at birth	0
Age at death	0
APOE genotype	27
Educational degree	0
Neighborhood median household income	1
Race	0
Ever smoker	2
Regular exercise	2
Body mass index category	2
Diabetes	3
Hypertension	6
Cardiovascular disease	10

Table 4: Complete cases classified by clinically significant CERAD and Braak scores.

	Braak significant	Braak not significant	Total
CERAD significant	223	121	344
CERAD not significant	32	232	264
Total	255	353	608

Table 5: Autopsy complete cases with both Braak and CERAD clinically significant versus clinical diagnosis of dementia

	Both Braak and CERAD significant	Both Braak and CERAD not significant	Total
Clinical dementia	172	128	300
Clinical no dementia	51	257	308
Total	223	385	608

Pearson's Chi-squared test with Yates' continuity correction:

Chi-square = 107, df = 1, p-value <0.0001

Figure 1: National Institute on Aging and Reagan Institute (NIA-RI) consensus recommendations on clinical correlation with Braak staging and CERAD scores.

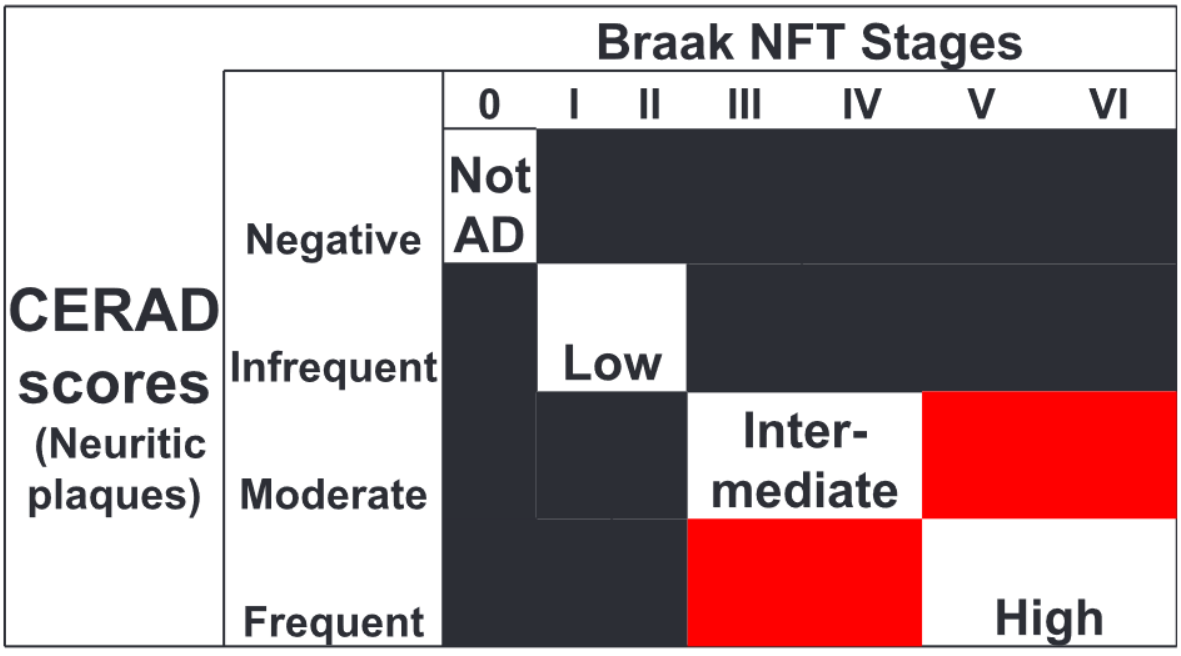

Figure 2: Complete cases UFP exposure boxplot

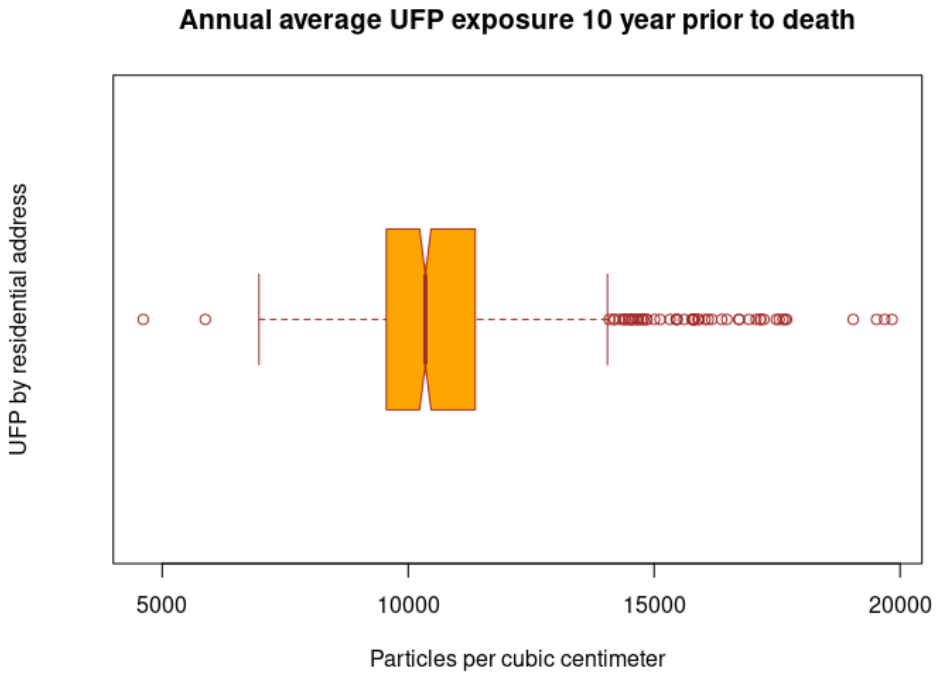

Figure 3: Complete cases both CERAD and Braak clinically significant versus UFP exposure boxplot

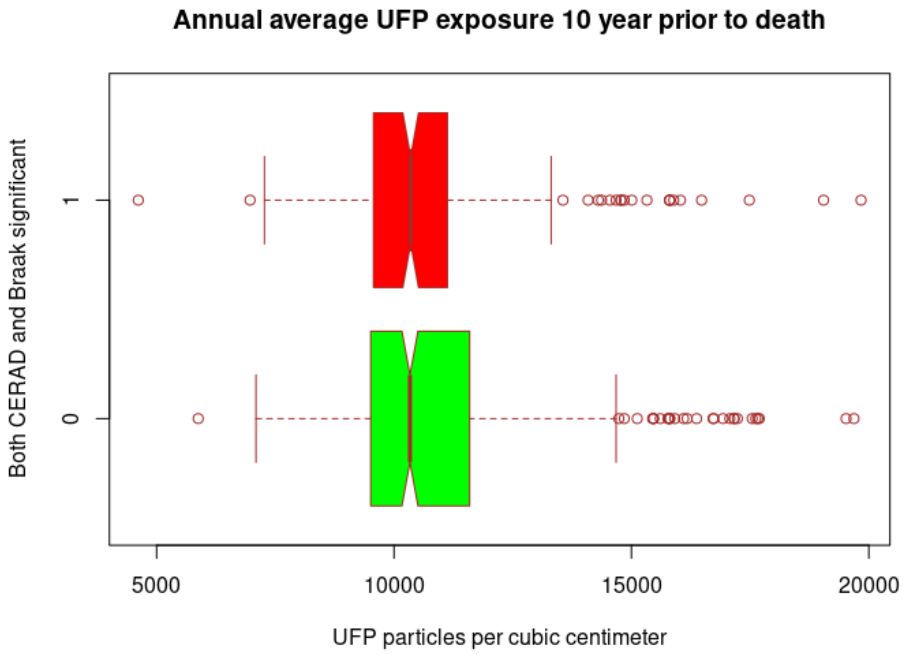

Figure 4: Complete cases CERAD scores clinically significant versus UFP exposure boxplot

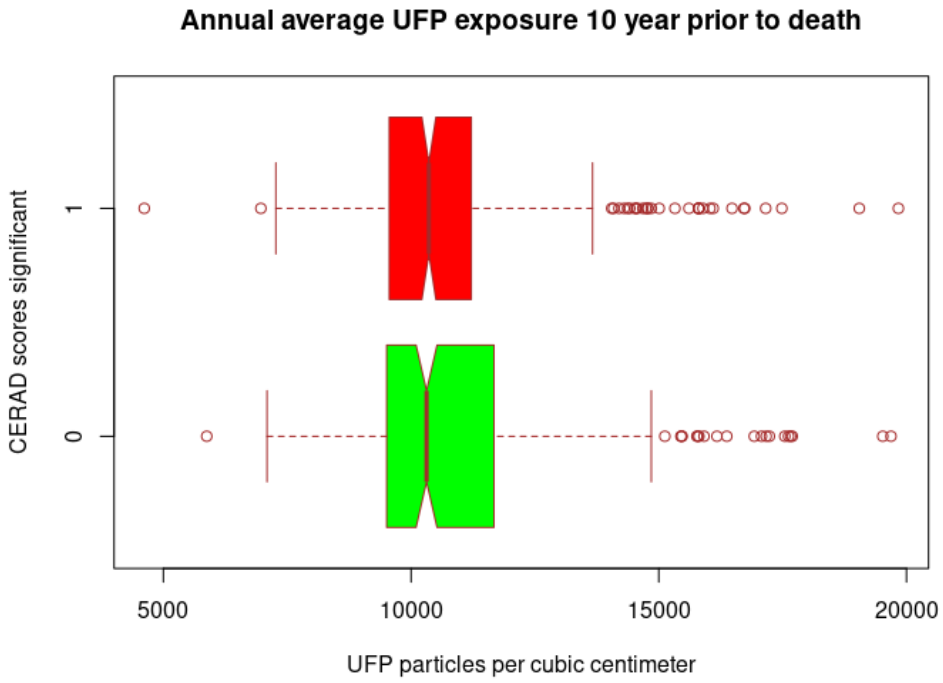

Figure 5: Complete cases Braak staging clinically significant versus UFP exposure boxplot

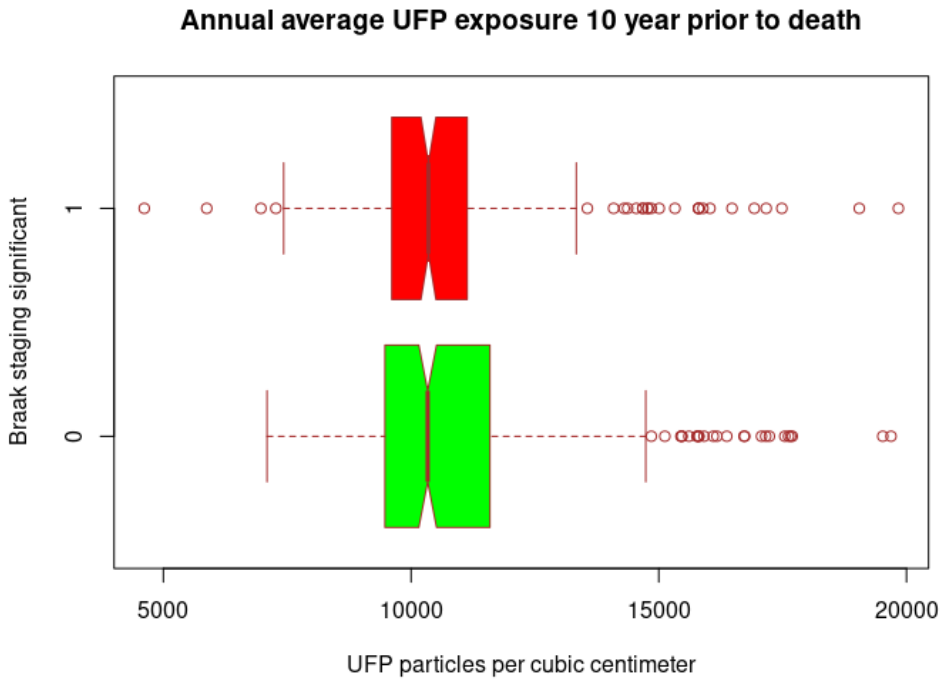

SECTION TWO: A case study to establish research methodology to enhance ACT spatial model UFP exposure prediction near high emission source, such as SEATAC airport, using AERMOD modeling.

INTRODUCTION:

We have selected ACT spatial model air sampling sites to be in proximity to individuals' residential addresses. Incidentally, ACT spatial model captures the location of high polluting sources, including SEATAC airport. Knowing the emission distribution of high polluting sources in higher resolution may help researchers to plan health interventions. In our aim 2, we will investigate using AERMOD to model UFP emission distribution contributed by SEATAC aircraft traffic flow.

Monitoring campaigns in Seattle, Los Angeles, Atlanta, Boston, New York, and Amsterdam all found higher UFP pollution near the airports [69-76]. Aircraft traffic flow UFP emission distribution can be an insightful covariate to be added to ACT spatial model by future researchers.

We use AERMOD because it is accepted by the Environmental Protection Agency (EPA) and Federal Aviation Administration (FAA) [25,26].

Traditionally, AERMOD has been used to simulate stationary polluting sources [77]. Dr. Larson has used AERMOD to simulate aircraft traffic flow pollutions in his previous papers [71-73]. In this study, we made parameter adjustments suitable for SEATAC airport, but we used the same model parametrization applied previously by Dr. Larson.

We hypothesize that our aim 2 methodology will improve our spatial understanding of the impact of UFP emissions and allow our UFP models to better capture impact of emissions related to SEA-TAC aircraft traffic flows. Our methodology can also be used to help to plan the optimal location to collect air samples for ACT or other air quality monitoring studies.

Overlaying AERMOD emission distribution onto ACT spatial model may give us a more accurate exposure predictions and thus illuminate a possible association between UFP and AD neuropathology. We are not attempting the enhancement of ACT spatial model using the AERMOD output in this thesis; this work will be completed by other team members in the future.

METHODS:

Modeling Concept:

AERMOD simulates air pollution emission distribution within an integrated graphic user interface called AERMOD view. AERMOD uses time-stamped meteorological and terrain data inputs in its simulation. Therefore, AERMOD simulation always has a temporal component. In addition, AERMOD view spatial component includes latitude and longitude coordinates, terrain features with geographic position system (GPS) identifiers and land use surface roughness. The incorporation of these data input in air quality model assessment are specified by EPA in 40 CFR (Code of Federal Regulations) 51.112, 51.117, 51.150, 51.160, 51.165, 51.166, 52.21, 93.116, 93.123, and 93.150 [26,81]. Please see Appendix for detailed set-up parameters.

We are free to pick our air pollution emission sources and pollution receptors within the user interface. Because AERMOD view is paired with the graphic information system (GIS) and synced with Google map, the location of the emission sources and receptors have matching UTM longitudinal and latitudinal coordinates, simulating real world locations. Figure 6 is an example of SEATAC airport, a real location displayed within AERMOD view. The longitude and latitude of the SEATAC area are framed on the edges.

The AERMOD receptors provide emission distribution values. The receptor emission distribution values can be downloaded as an ADO text file. AERMOD view will smooth the

receptor values into a continuous spatial surface. The AERMOD spatial surface allows researchers to make emission prediction using a single air sample data point located within the distribution.

AERMOD incorporates modeled atmospheric boundary layer dynamics as well as 3-dimensional wind vectors to capture temporal differences in atmospheric conditions. A Gaussian dispersion model, which accounts for hourly boundary layer height, atmospheric stability and predominant wind direction is used to simulate the movement of emissions from the source to the receptor locations. AERMOD conducts Gaussian dispersion model as follows. AERMOD averages an array of many plumes based on meteorological data in year 2019. Certain plume patterns within the array occur more frequently based on Gaussian distribution (a normal distribution). EPA accepts the predictions from Gaussian dispersion models [81].

AERMOD view simulates an upper atmosphere and a lower atmosphere, which behave as two independent layers of gas. AERMOD simulates friction at the boundary layer which slows down gas mixing between the layers. The upper and lower atmosphere are highly pertinent independent variables for the distribution of air pollution. AERMOD further simulates distribution in relation to terrain, surface land use, and surface to lower atmospheric friction [26].

We select the maximum UFP emission at the emission source to be 1 microgram per cubic centimeters. This maximum UFP emission can be set to be any number because we are only interested in the relative spatial distribution. Carbon dioxide emission is selected as the surrogate emission type to simulate UFP because of UFP's small particle size and therefore negligible deposition rate.

We use a rectangular receptor grid with receptors spaced 1 kilometer equidistance apart (Figure 6). The grid size is 86 kilometers longitudinally and 40 kilometers latitudinally. More

receptors require more computation power and thus longer computation time. After my own experimentation, any distance smaller than 1 kilometer does not appear to make a difference in plume spatial resolution. We design to use a large receptor grid to capture where the distribution of SEATAC UFP density drops to 0.1% of the maximal emission. The grid has 1743 receptors.

The rectangular receptor grid is centered at the mid-distance of the SEATAC airport runway number 3. We design the length of the receptor grid to be parallel to longitude and the width of the grid to be parallel to latitude. This design allows our grid to be transferrable to other geographic spatial programs. All the runways of SEATAC are incidentally parallel to the longitude, and they are closely collocated (Figure 6). Therefore, we decided to model all the traffic flow using only one runway, since the traffic flow directions and common flight path locations are relatively similar among all runways.

We model aircraft traffic to reflect 2019 FAA traffic records as closely as possible. The directions of landing and takeoff are usually predetermined by wind directions because aircrafts will gain additional amount of lift when flying against the direction of the wind. Landing aircrafts are directed to fly into the wind to touch down softly. During takeoffs, aircrafts fly into the wind to be blown up into the sky. Because the average wind direction changes seasonally, two thirds of all calendar days in 2019 had unidirectional flow within a 24-hour period. This 24-hour unidirectional flow pattern allows us to simplify SEATAC air traffic flow simulation into four independent simulations: south flow landing, south flow takeoff, north flow landing, and north flow take off.

All four simulations use the same receptor grid to calculate their UFP emission distributions. Each simulation results in a separate UFP emission distribution. South flow traffic is defined by aircrafts flying longitudinally toward the geographic south pole of the Earth. North

flow traffic is defined by aircrafts flying longitudinally toward the geographic north pole of the Earth.

The range of dates for all four simulations fall somewhere between 1JAN2019 to 31DEC2019. We run simulations only on calendar days with unidirectional flow. Calendar days with mixed traffic flow are not used because we have large number of unidirectional flow days. Figure 7 shows the calendar days for both south flow landing and south flow takeoff simulations. Figure 8 shows the calendar days for both north flow landing and north flow takeoff simulations.

We use year 2019 meteorological data for lower and upper atmosphere from National Oceanic and Atmospheric Association (NOAA). We use the nearest air sample monitors to the SEATAC airport, Quillayute upper atmosphere monitoring station and SEATAC airport surface monitoring station. Please see APPENDIX for setting details.

We use ground-level elevation and terrain data provided by National Elevation Dataset (NED) into AERMOD. See APPENDIX for setting details.

Hourly variation in traffic density is simulated by a 24-hour table of annual average percentage for landing (Table 6) and for takeoff (Table 7).

We design our flight paths based on the final common flight paths provided by FAA. The south flow landing simulation flight path ends at ground level at the northern end of SEATAC runway 3. The south flow landing simulation flight path starts at the 1000-meter elevation with a 20-kilometer horizontal distance. The landing angle is 3 degrees. Therefore, the horizontal distance for the start of the flight path is 20 kilometers when the starting elevation is 1000 meters. 1000-meter starting elevation is always above the boundary layer. The daily heights of the boundary layer for the year 2019 are documented by the NOAA meteorological data. Aircraft UFP pollution released above the boundary layer is dispersed wide and in low

density, while UFP pollution released below the boundary layer is focally impacted on to the ground. AERMOD simulates the distributive effect of both upper and lower atmosphere. The north flow landing simulation flight path is a mirror image of the south flow landing simulation flight path.

The south flow takeoff simulation flight path starts at ground level at the southern end of SEATAC runway 3. The takeoff angle is 10 degrees. The ending elevation is 1000 meters and horizontal distance is 5671. North flow takeoff simulation flight path is the mirror image of the south flow takeoff simulation flight path.

We use line-volume sources in our flight path simulations. A line-volume source is a series of volume cubes where AERMOD allows for air mixing within the cubes before the release of pollution. We set the sides of the volume cube to be 50 meters to simulate the wake turbulence generated by the aircraft wings because the distance between the wing tips for a typical commercial aircraft is approximately 50 meters.

All simulations performed on Lakeview AERMOD version 10.2.1 [83].

RESULTS:

Descriptive statistics:

159 days in the year 2019 had only south flow traffic, which are used in both south flow landing and takeoff simulations (Figure 7). 37 days in the year 2019 had only north flow traffic, which are used in both north flow landing and takeoff simulations (Figure 8). SEATAC airport used south flow traffic 72% of all hours in the year 2019. South flow traffic was used in all months of the year 2019, while north flow traffic was not used at all during the months of October and December in 2019.

Figure 9 shows the result of our south flow landing simulation. This figure shows the percentage of aircraft emissions simulated to occur within each grid cell; the percentages are on a logarithmic scale and range from 0.1% to 100%. Exposure is highest right under the flight paths. The 90% emission area is within 1 kilometer distance of the fight path. The wind pushes emission distribution asymmetrically toward the north, while the east and west UFP emission distributions are symmetrical.

In our south flow takeoff simulation (Figure 10), the ground UFP emission has a smaller footprint when compared to the south flow landing simulation. The emission distribution of south flow takeoff simulation is less than one four the size of the south flow landing simulation. The smaller south flow takeoff footprint is consistent with aircrafts traveling a shorter distance below the boundary layer during takeoff. The emissions percentage is at 90% within 500 meters of the horizontal distance to the flight path. The wind pushes UFP emission distribution asymmetrically toward the north of the airport, while the east and west UFP emission distributions are symmetrical.

Figure 11 shows the result of our north flow landing simulation. The wind pushes the distribution toward the south and west. The distribution size of the north flow landing simulation is half of the south flow landing simulation.

Figure 12 shows the result of our north flow takeoff simulation. The wind pushes the distribution toward the south and west. The distribution size of the north flow takeoff simulation is half of the south flow take off simulation. Figure 13 shows all four simulations in the same frame for comparison.

DISCUSSION:

Our AERMOD SEATAC aircraft traffic flow UFP emission simulations suggest the most impacted communities are directly under the flight paths when aircrafts fly below the boundary layer (Figure 9). Our AERMOD simulations demonstrate high pollution peaks and sharp reductions of UFP as a function of distance from the flight path.

While we have not combined the output of our four simulations into one using weighted ratio, we can make predictions with our current progress. Both south flow landing and south flow takeoff traffic simulations show the area immediately north of the SEATAC airport is highly impacted. ACT spatial model shows the area north of SEATAC airport has high UFP exposure when compared to the area south of SEATAC airport (Figure 14). Our AERMOD predictions may have implications for the health of people north of SEATAC and south of Seattle downtown.

We recommend future researchers to use the output of our AERMOD model as a covariate in ACT spatial model. We expect that a revised ACT spatial model that includes an AERMOD covariate will result in a reduced width of the confidence interval in our aim 1 by increasing precision of the exposure prediction.

The cost of the AERMOD software is low when compared to the labor and equipment cost of air samples. AERMOD has the potential to reduce the total number of air samples needed to achieve high resolution spatial model. Approximately 150 student-hours were invested in developing the methodology detailed in the Appendix. We expect new students to learn the methodology quickly using this thesis.

If SEATAC air traffic highly impacts the health of the population living between SEATAC and downtown Seattle, then SEATAC airport is disproportionately impacting people who identify with being minority, living below poverty line, and without high school diploma

(Figure 15, 16, 17) [78]. This population is less likely to mitigate air pollution by purchasing and using air filters and air conditioning. Our study can be used to advocate for the people who are vulnerable and paying the high price of economic development for Puget Sound through their health.

CONCLUSION:

We have demonstrated that AERMOD is capable of modeling aircraft traffic flow UFP pollution. AERMOD is a low-cost method to gain insight on high polluting source. AERMOD can be a useful tool to plan air sample collection sites. Our AERMOD simulations suggest SEATAC aircraft traffic may lead to focally elevated UFP exposure for people living under the flight paths. Future research should incorporate these AERMOD predictions into a revised ACT spatial model. The implications of this work may extend far beyond this case study to improve UFP exposure predictions around airports in other areas.

Figure 6: SEATAC airport inside AERMOD view. UTM East longitude ruler and UTM North ruler on the edges. The runway on the most west is runway 3. The runway in the middle is runway 2. The runway on the east is runway 1.

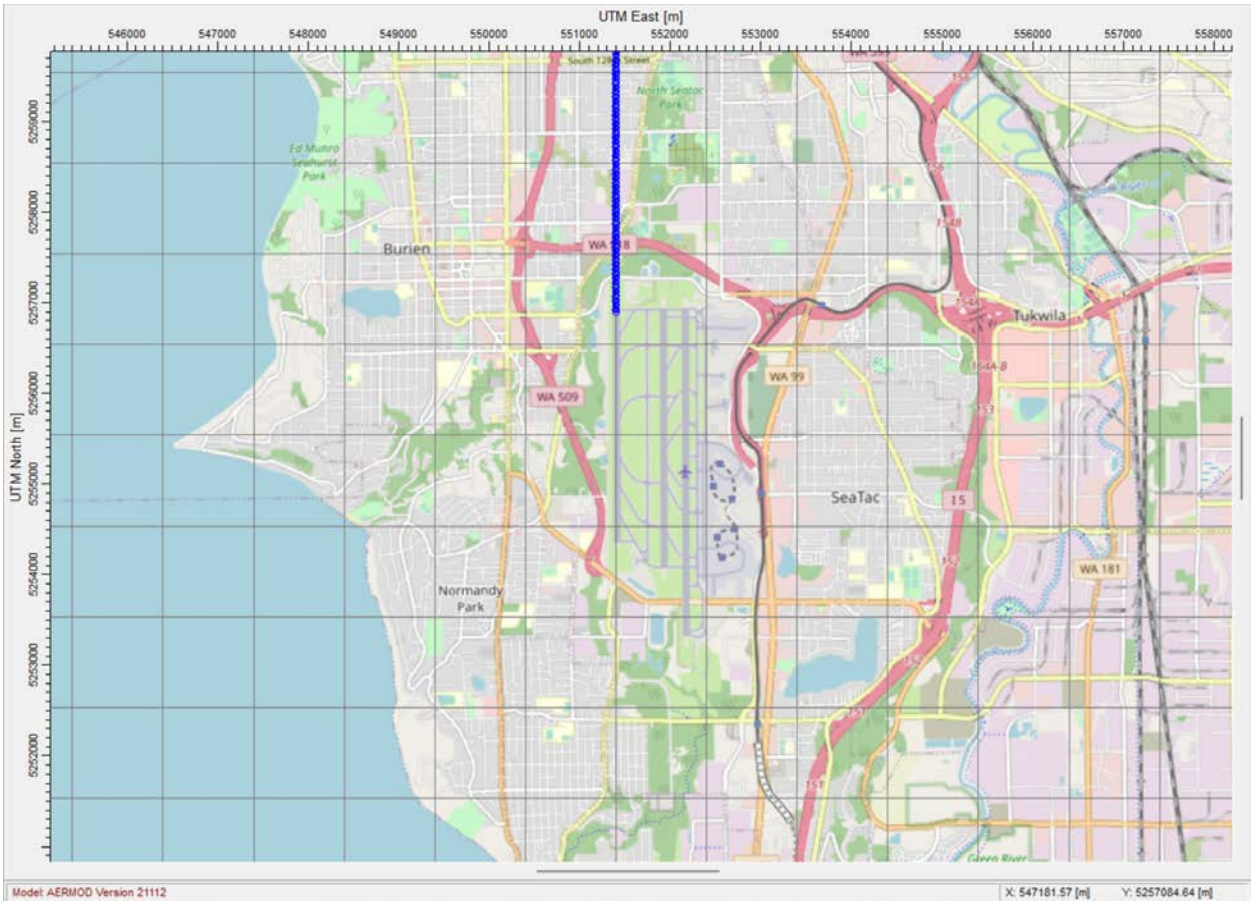

Figure 7: The calendar days for both south flow landing and south flow takeoff simulations

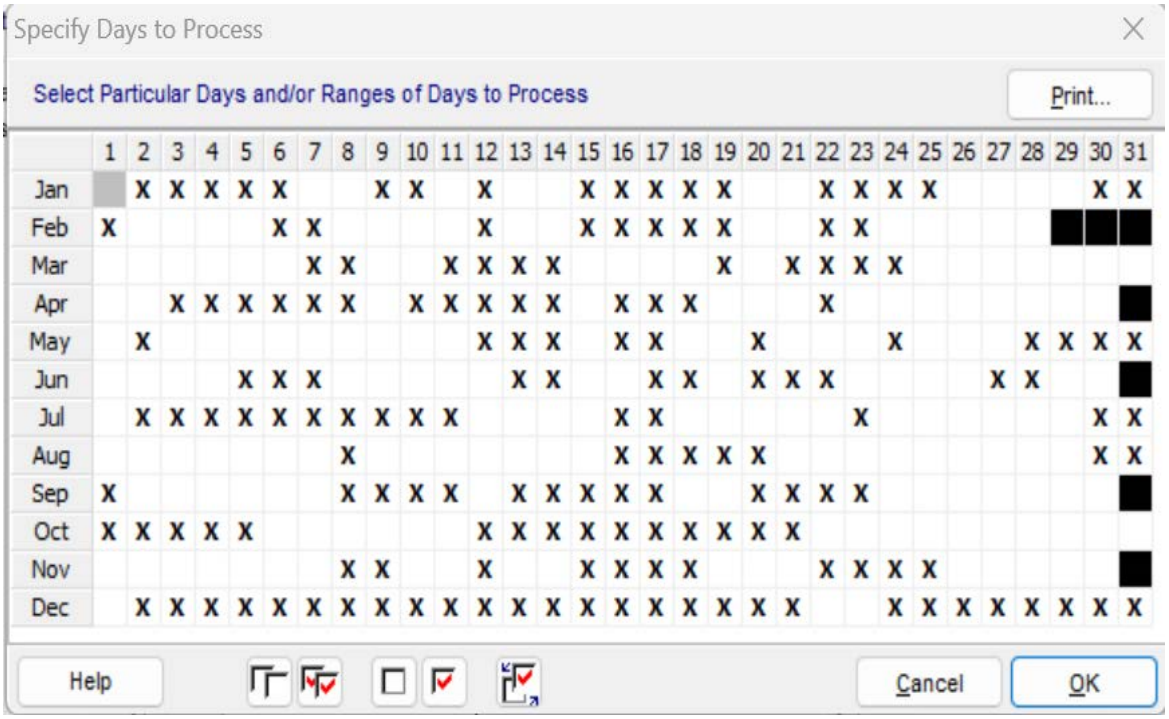

Figure 8: The calendar days for both north flow landing and north flow takeoff simulations

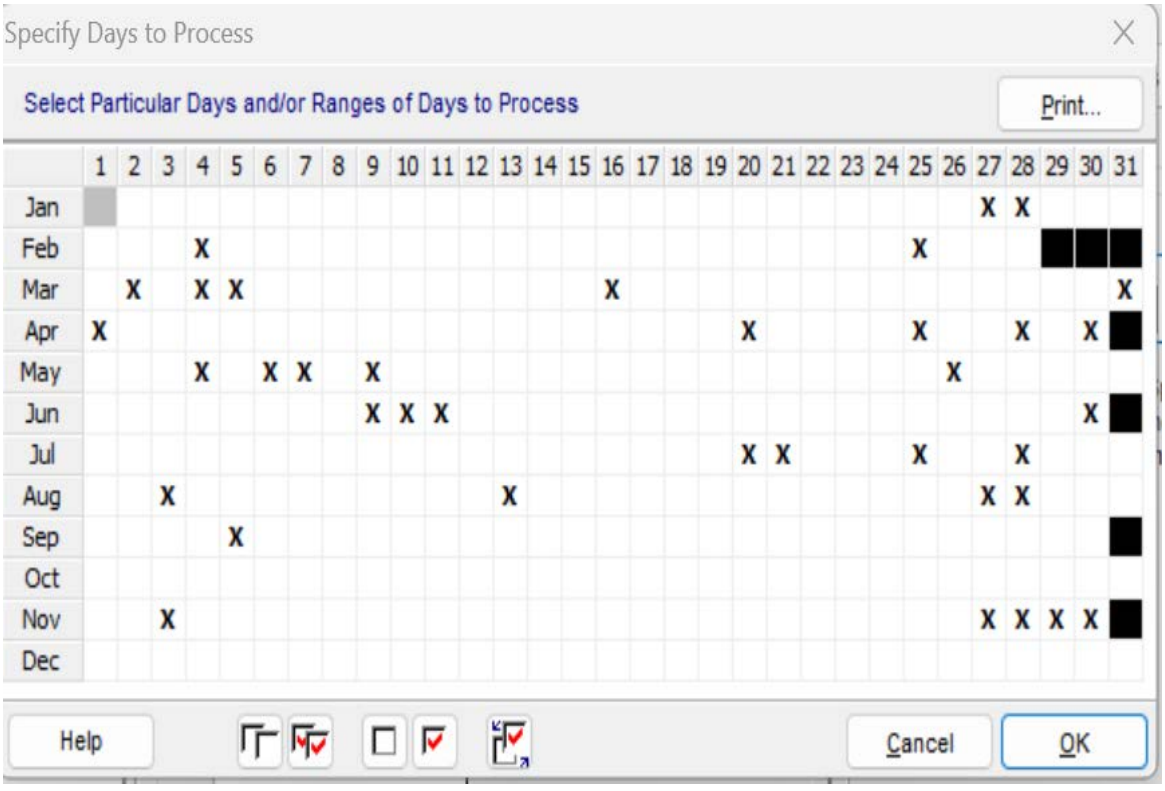

Figure 9: South flow landing simulation output. Each square is 1000 meters x 1000 meters.

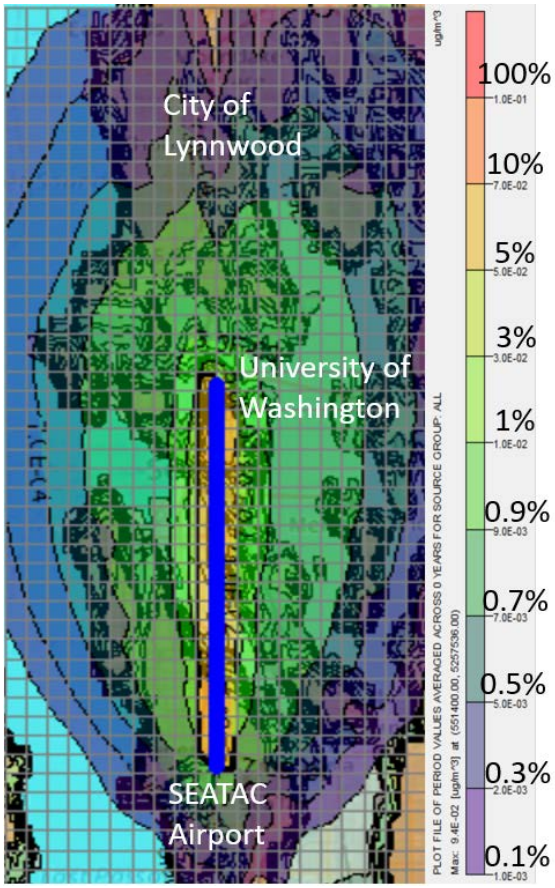

Figure 10: South flow takeoff simulation output. Each square is 1000 meters x 1000 meters.

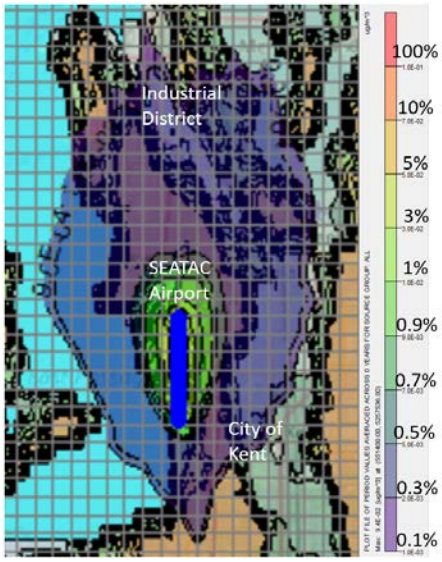

Figure 11: North flow landing simulation output. Each square is 1000 meters x 1000 meters.

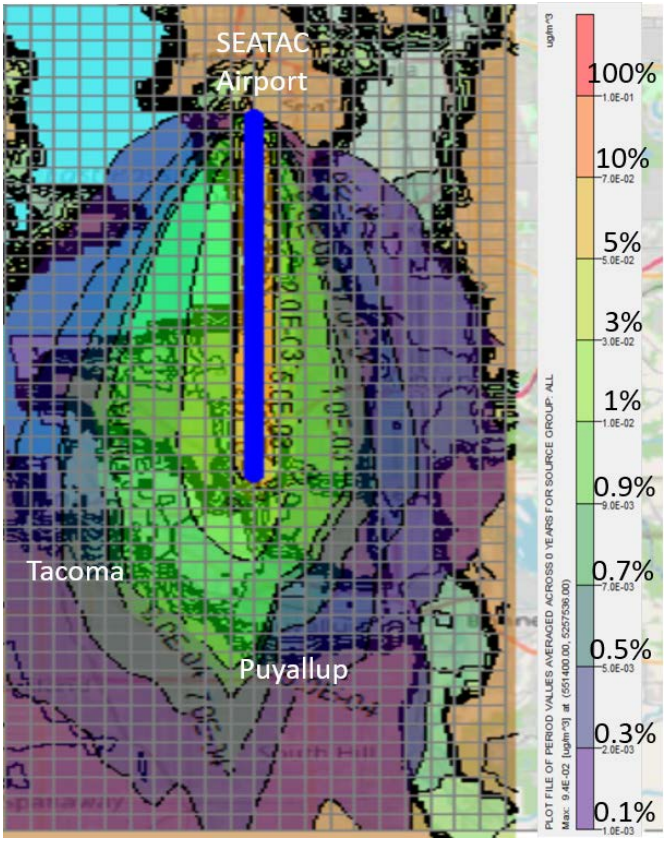

Figure 12: North flow takeoff simulation output. Each square is 1000 meters x 1000 meters.

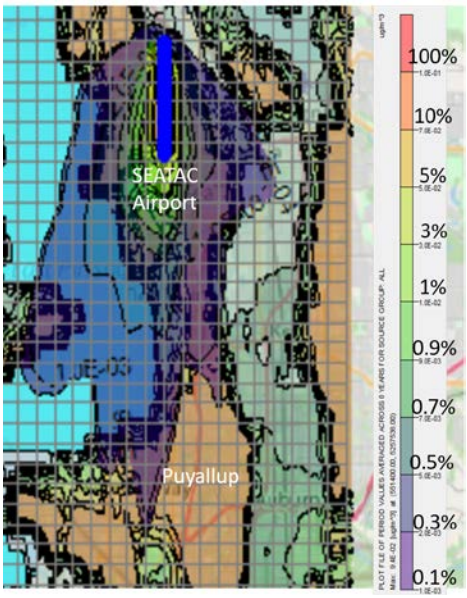

Figure 13: Simulation same frame comparison.

South flow landing	South flow takeoff
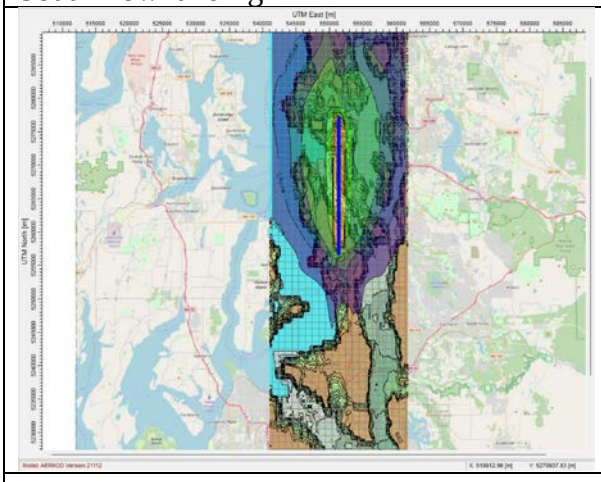	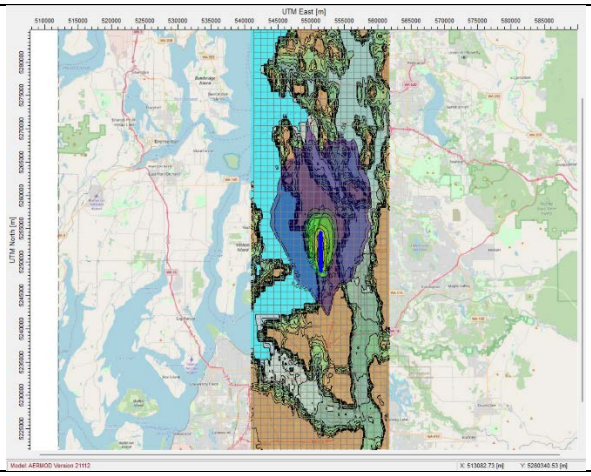
North flow landing	North flow takeoff
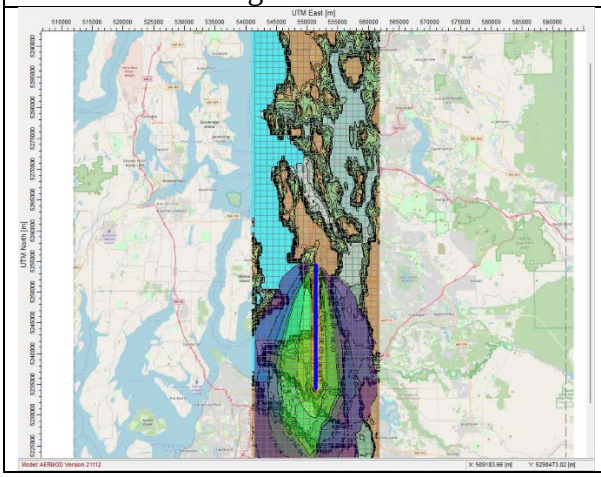	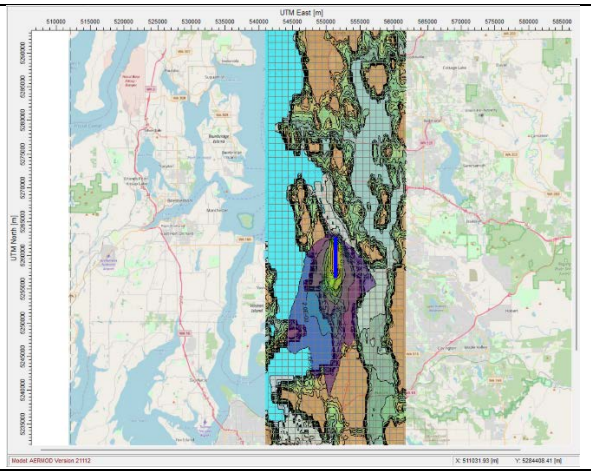

Table 6: Annual average hourly density for landing

Hour	Hourly Contribution (%)
0	0.011823
1	0.005653
2	0.00322
3	0.002534
4	0.009014
5	0.017786
6	0.037937
7	0.025769
8	0.064454
9	0.057037
10	0.067236
11	0.049898
12	0.060456
13	0.044156
14	0.062937
15	0.043621
16	0.062459
17	0.051463
18	0.0508
19	0.061066
20	0.068833
21	0.065967
22	0.05088
23	0.025

Table 7: Annual average hourly density for takeoff

Hour	Hourly Contribution (%)
0	0.015825852
1	0.006597897
2	0.002338841
3	0.000445927
4	0.000646139
5	0.015484581
6	0.049952905
7	0.054630586
8	0.072676972
9	0.047741472
10	0.072626919
11	0.057287946
12	0.069691992
13	0.055763604
14	0.055731752
15	0.052692169
16	0.051427193
17	0.052655767
18	0.053324658
19	0.047354698
20	0.037990235
21	0.048182848
22	0.036424941
23	0.042504107

Figure 14: Locations of ACT UFP elevation

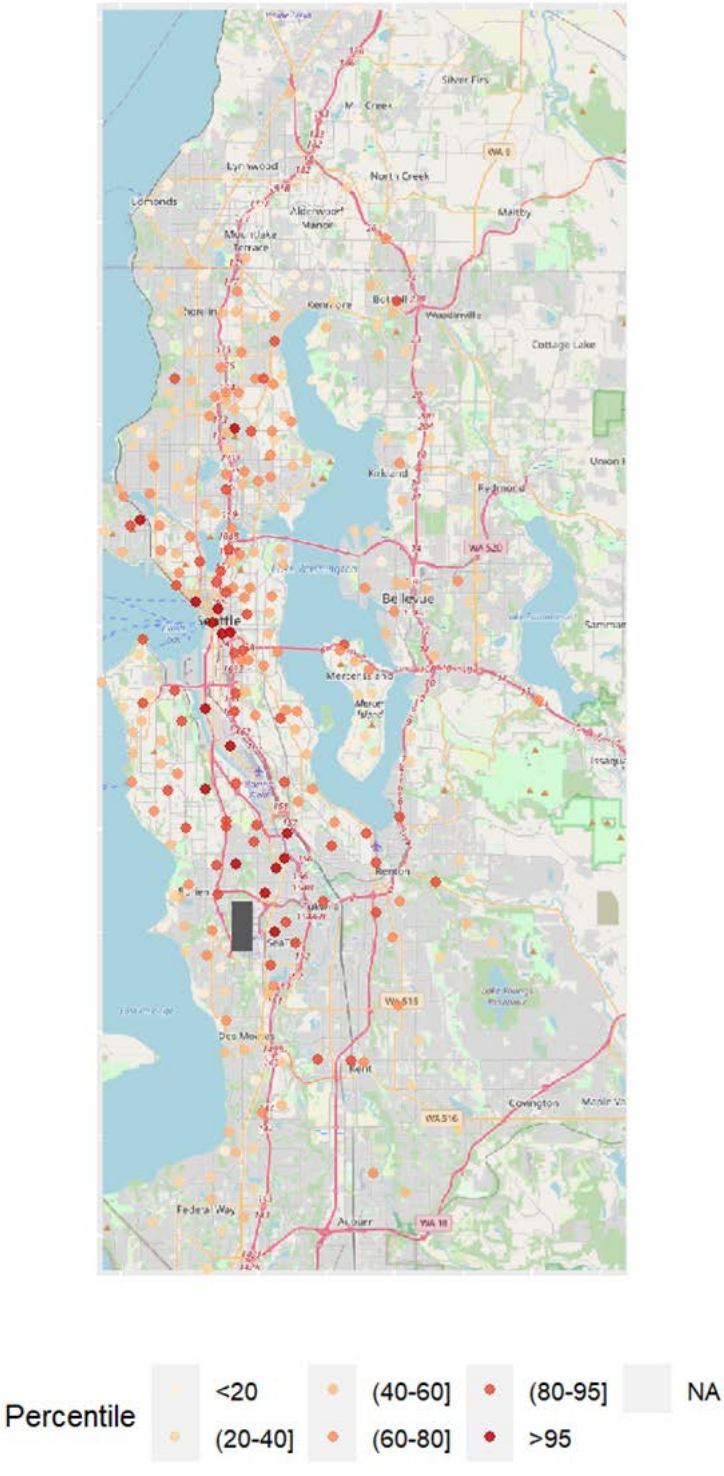

Figure 15: Washington State Environmental Justice Map Poverty Layer. The area outlined in yellow is SEATAC airport. AERMOD predicts the red rectangle area has elevated UFP related to SEATAC airport.

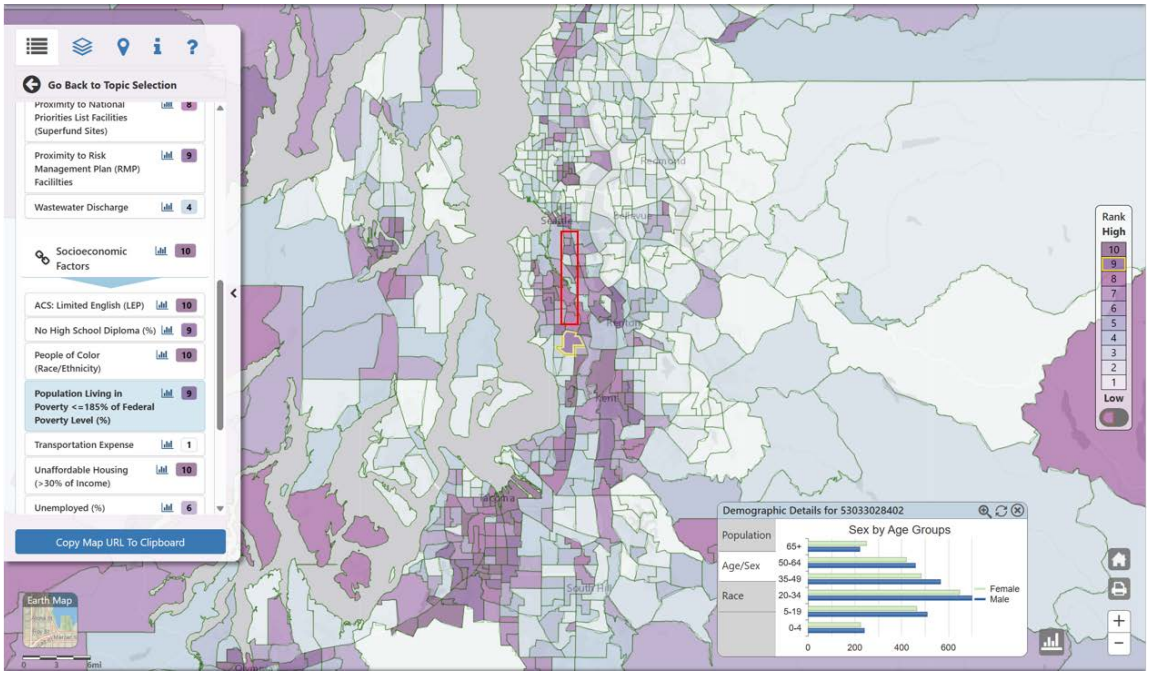

Figure 16: Washington State Environmental Justice Map no high school diploma. The area outlined in yellow is SEATAC airport. AERMOD predicts the red rectangle area has elevated UFP related to SEATAC airport.

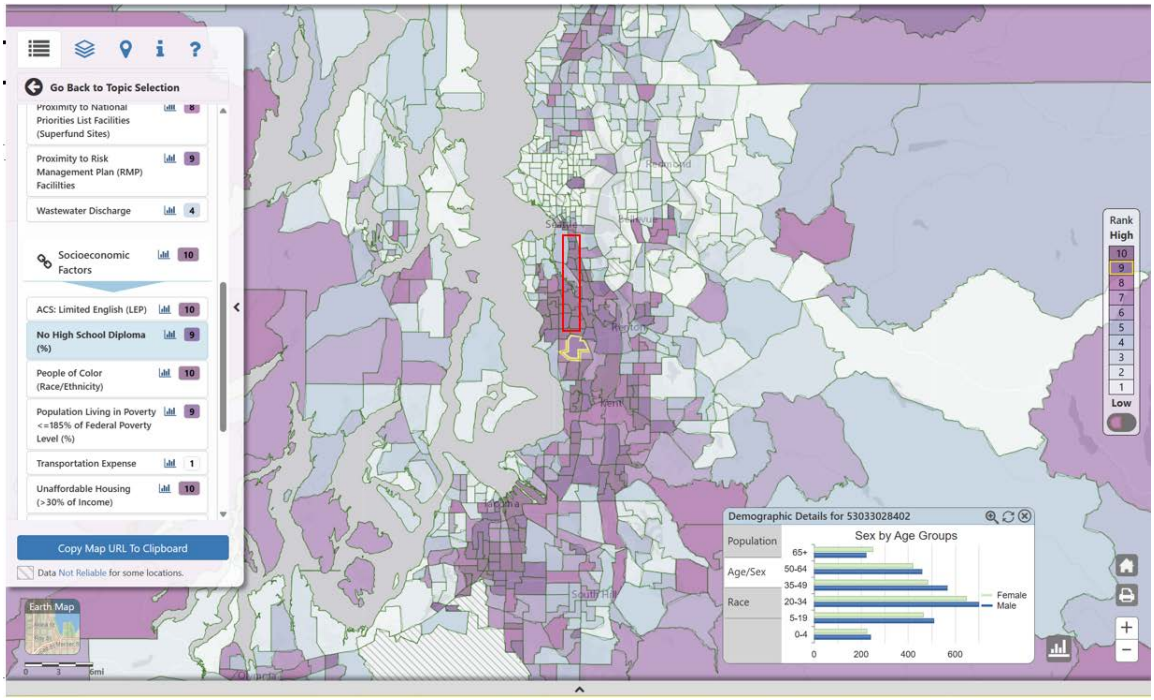

Figure 17: Washington State Environmental Justice Map minority. The area outlined in yellow is SEATAC airport. AERMOD predicts the red rectangle area has elevated UFP related to SEATAC airport.

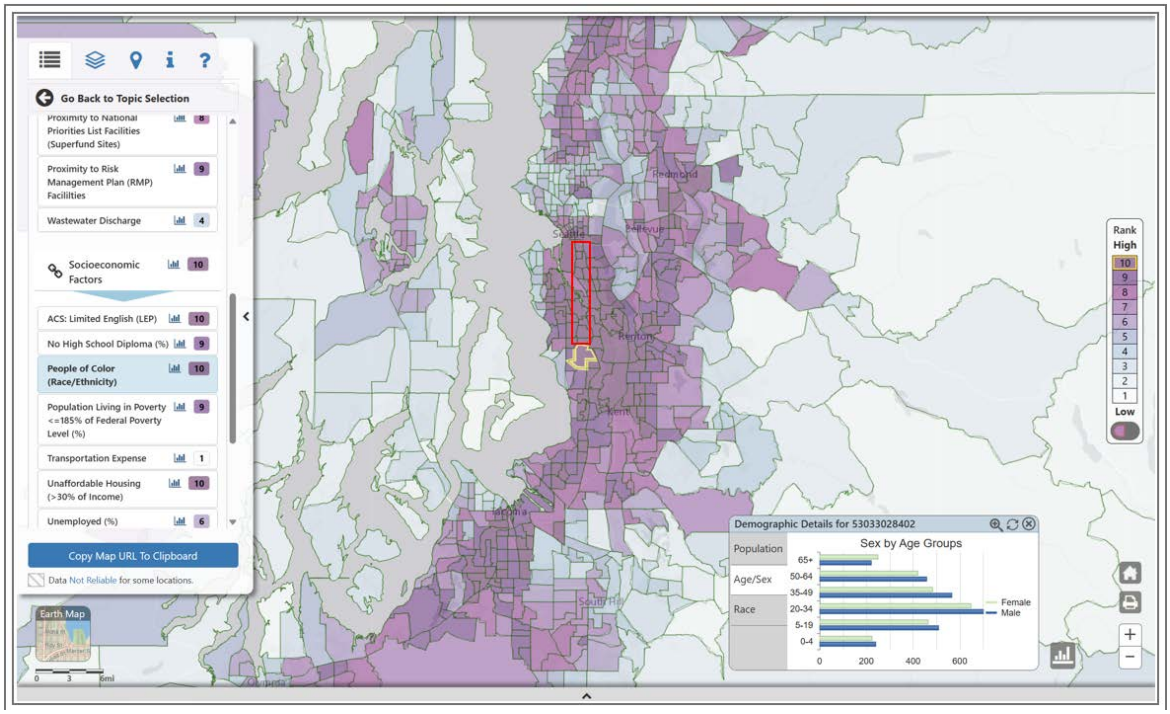

THESIS CONCLUSION:

In Aim 1, we found UFP may be associated with a wide range of effects on AD neuropathology. In Aim 2, AERMOD modeling predicts people living right under the SEATAC landing and takeoff aircraft flight paths may experience disproportionately elevated levels of UFP emitted by aircrafts. Future researchers should use AERMOD output and collect air samples under the flight paths as a covariate to enhance resolution of the ACT spatial model. Our research methodologies in both aim 1 and aim 2 provide new insights into strategies to model air pollution exposure based on roadway traffic, aircraft traffic, meteorological data, terrain, and land use data, as well as how to incorporate these predictions into inference about

health effects. Future work can build upon this research to advance our understanding of the potentially adverse effects of long-term UFP exposure on health outcomes.

APPENDIX: AERMOD settings for the analyses conducted under aim 2

Part A: AERMET settings:

AERMET is the program used to process meteorological data into formats that is used by AERMOD modeling. AERMET should be run before all other AERMOD programs.

PartA1: Downloading 2019 meteorological data:

You need to download meteorological data for both upper atmosphere and surface atmosphere from government websites before running AERMET.

PartA1a: Downloading 2019 Upper Atmospheric Data

Visit the following website: NOAA ERSL Radiosonde Database

https://ruc.noaa.gov/raobs/

Set Input dates for 2019. Select Stations/Data by State. (See snapshot below)

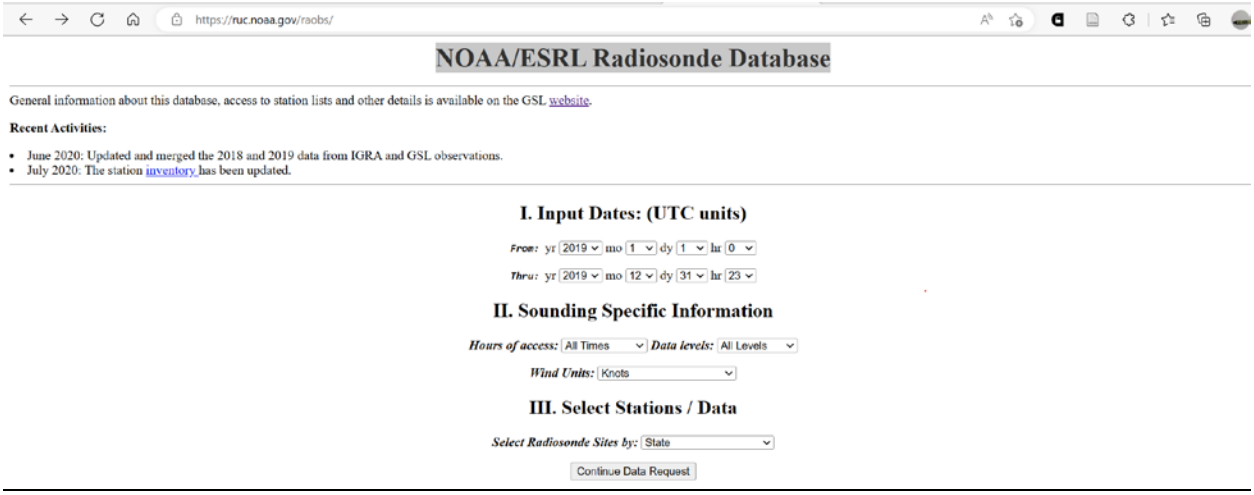

Access by State: Washington. View/select stations from states you have selected, choose Yes. (see snapshot below)

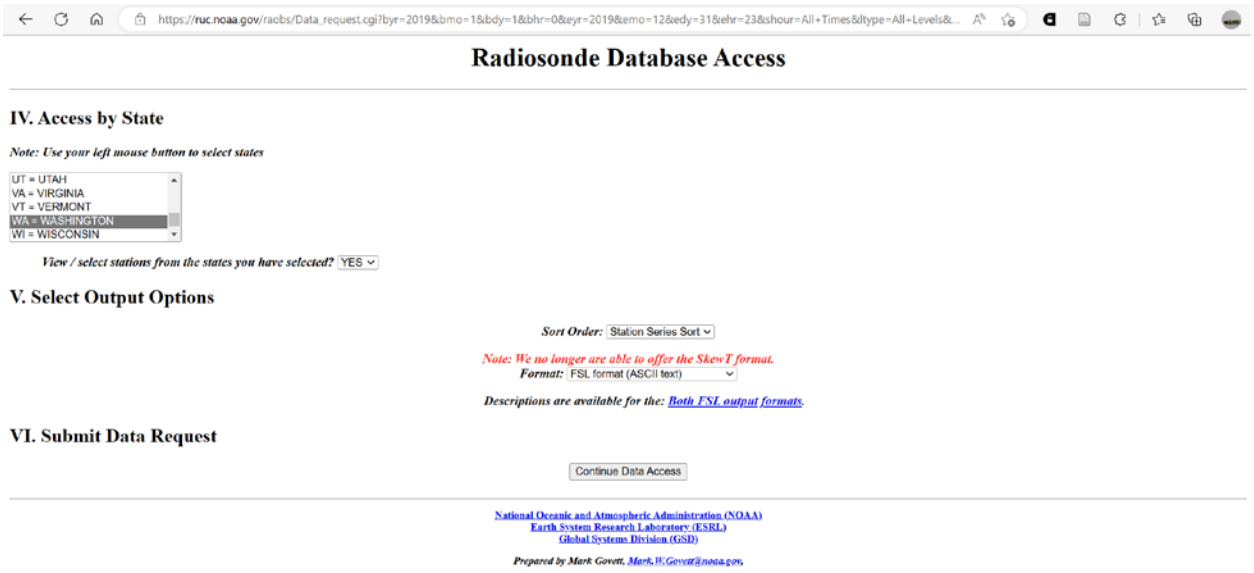

Click continue data access.

Choose Quillayute WA US because it is closest to SEATAC airport. (see snapshot below)

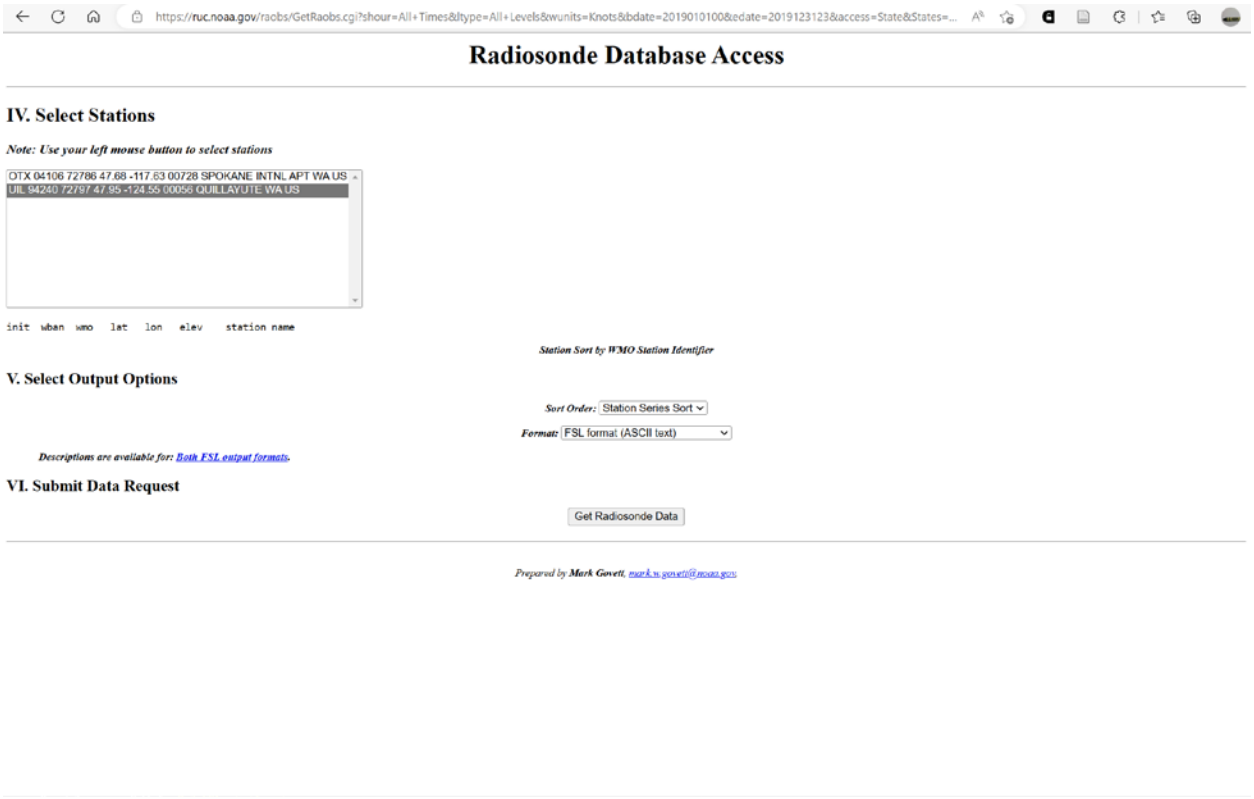

Keep format FSL format (ASCII text). Click Radiosonde Data.

Select all data by clicking in the Edge window, the Ctrl + A (see snapshot below).

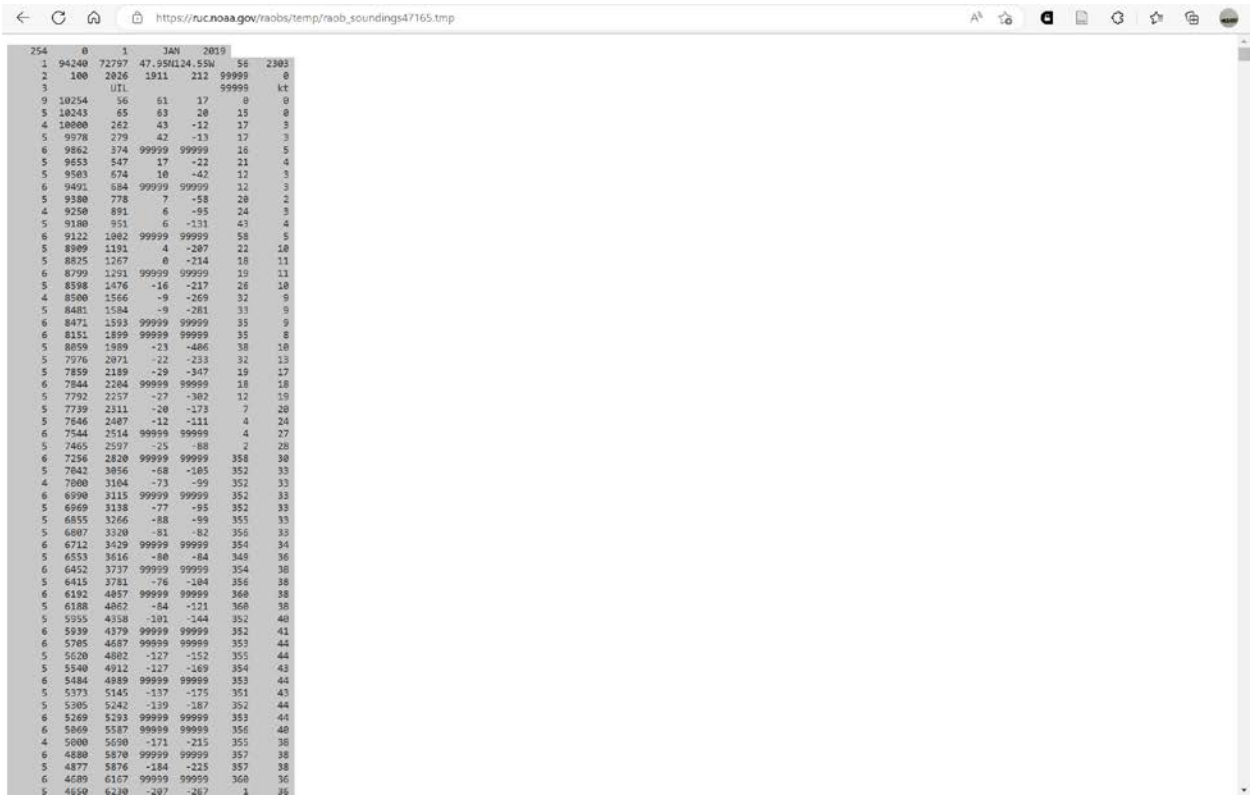

Open Wordpad. Copy Crtl+C and paste Crtl+V data into Wordpad.

Backspace until cursor is right to the last number in Wordpad. (see snapshot below)

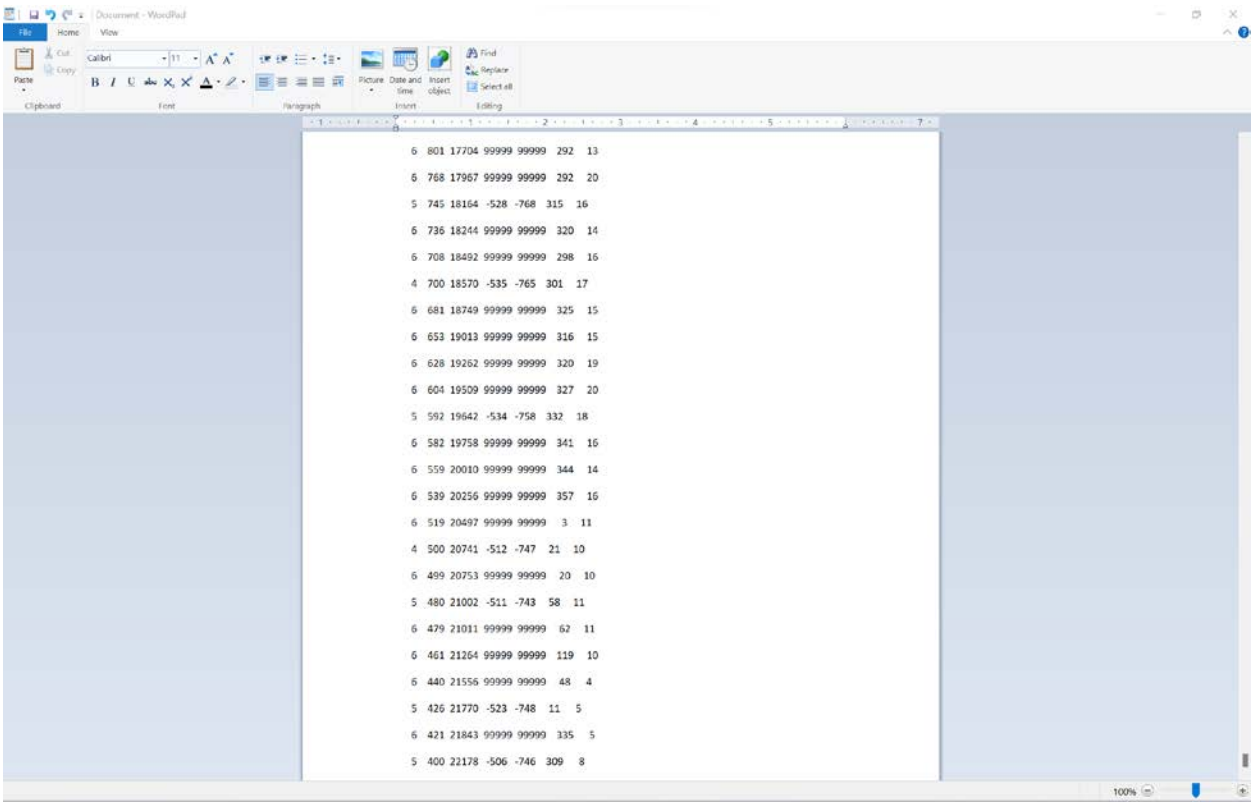

See filename as 2019.FSL. Save as type Text document (*.txt) to your project folder. (see snapshot below).

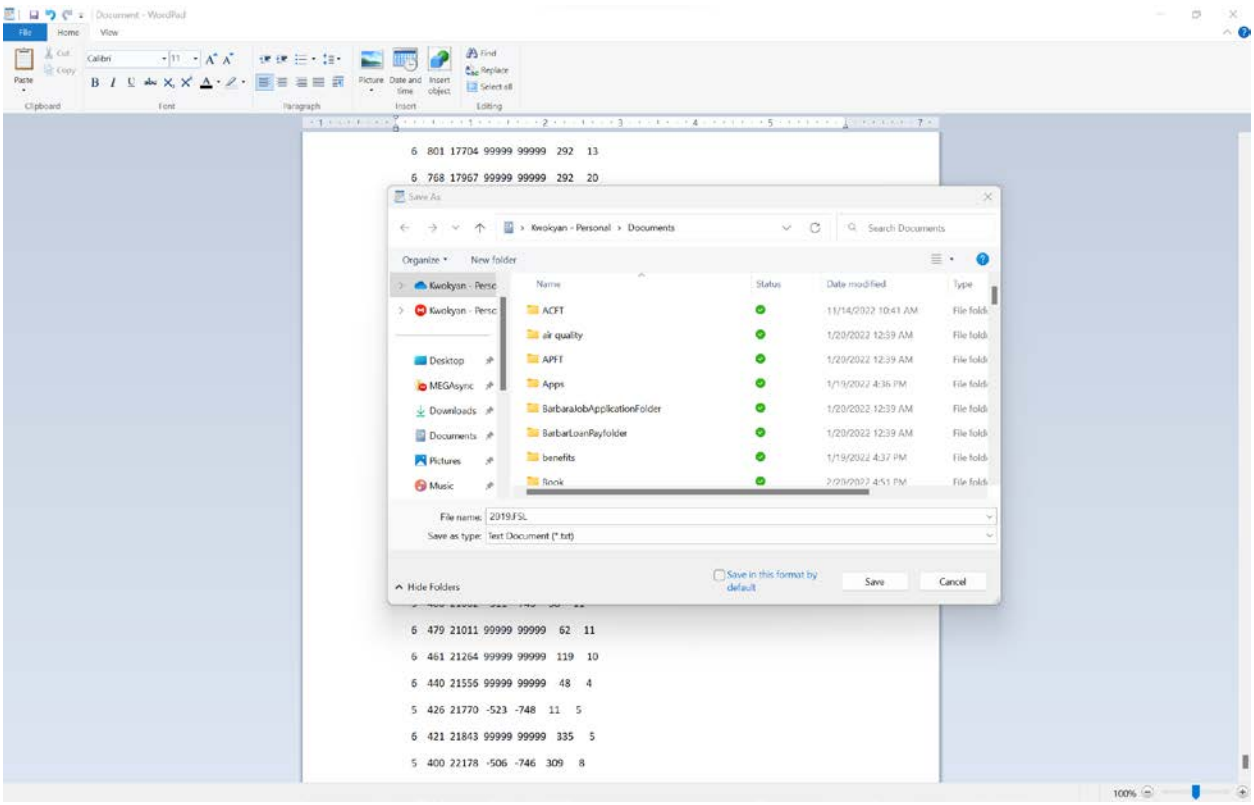

You have now downloaded 2019 upper atmosphere data and saved the data into 2019.FSL.

PartA1b: Downloading 2019 Surface Atmospheric Data

http://www1.ncdc.noaa.gov/pub/data/noaa/

Click on 2019 surface data. (see snapshot below).

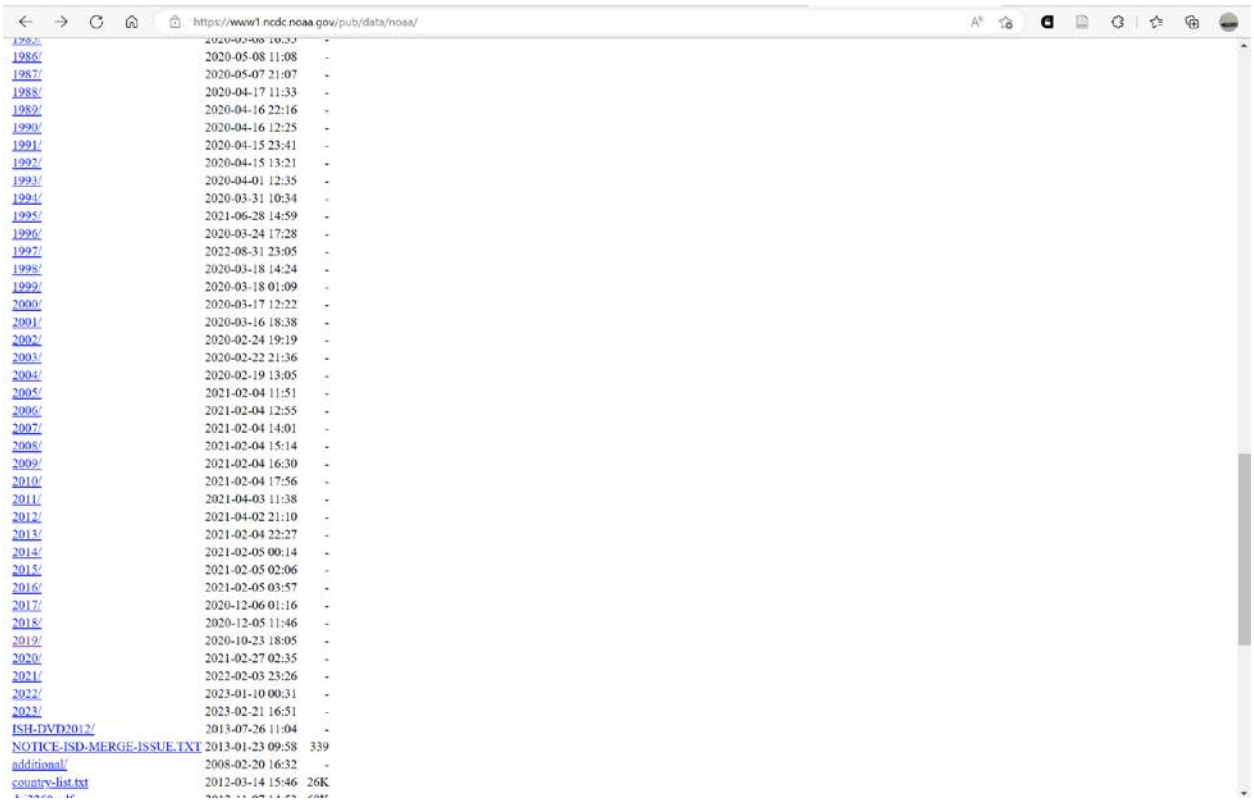

The surface station closest to SEATAC airport is 24233. Crtl+F to look for 24233. Choose the file 727930-24233-2019.gz, because that's the right one. (see snapshot below).

GZ file is a zip file. You will need an unzip program to unzip the file. 7zip is free.

The unzip ready to use file does not have .gz file extension. (see snapshot below).

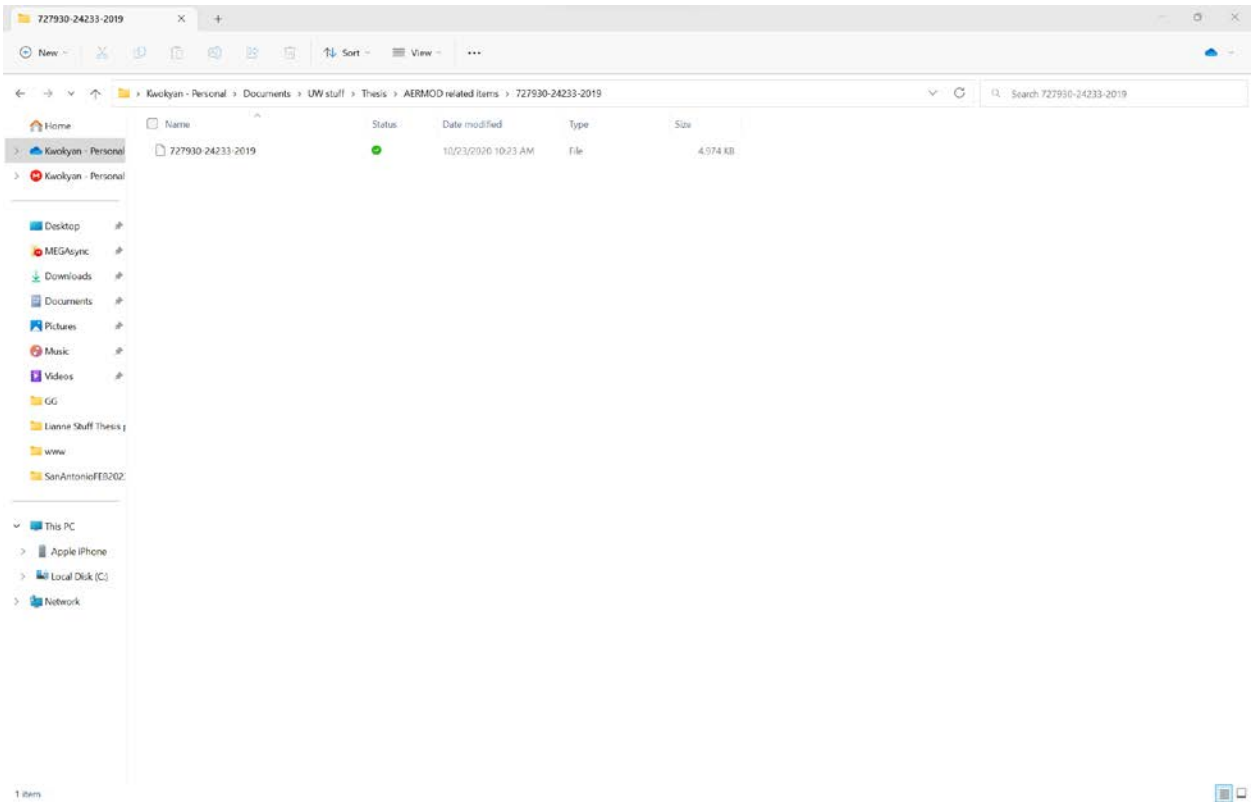
727930-24233-2019
New
Sort
View
Kwolyan - Personal › Documents › UW stuff › Thesis › AERMOD related items › 727930-24233-2019
Search 727930-24233-2019
Home
Kwolyan - Personal
Kwolyan - Personal
Desktop
MEGAsync
Downloads
Documents
Pictures
Music
Videos
GG
Lianne Stuff Thesis
www
SanAntonioFEB202
This PC
Apple iPhone
Local Disk (C:)
Network
Name
Status
Date modified
Type
Size
727930-24233-2019
10/23/2020 10:23 AM
File
4,974 KB
1 item

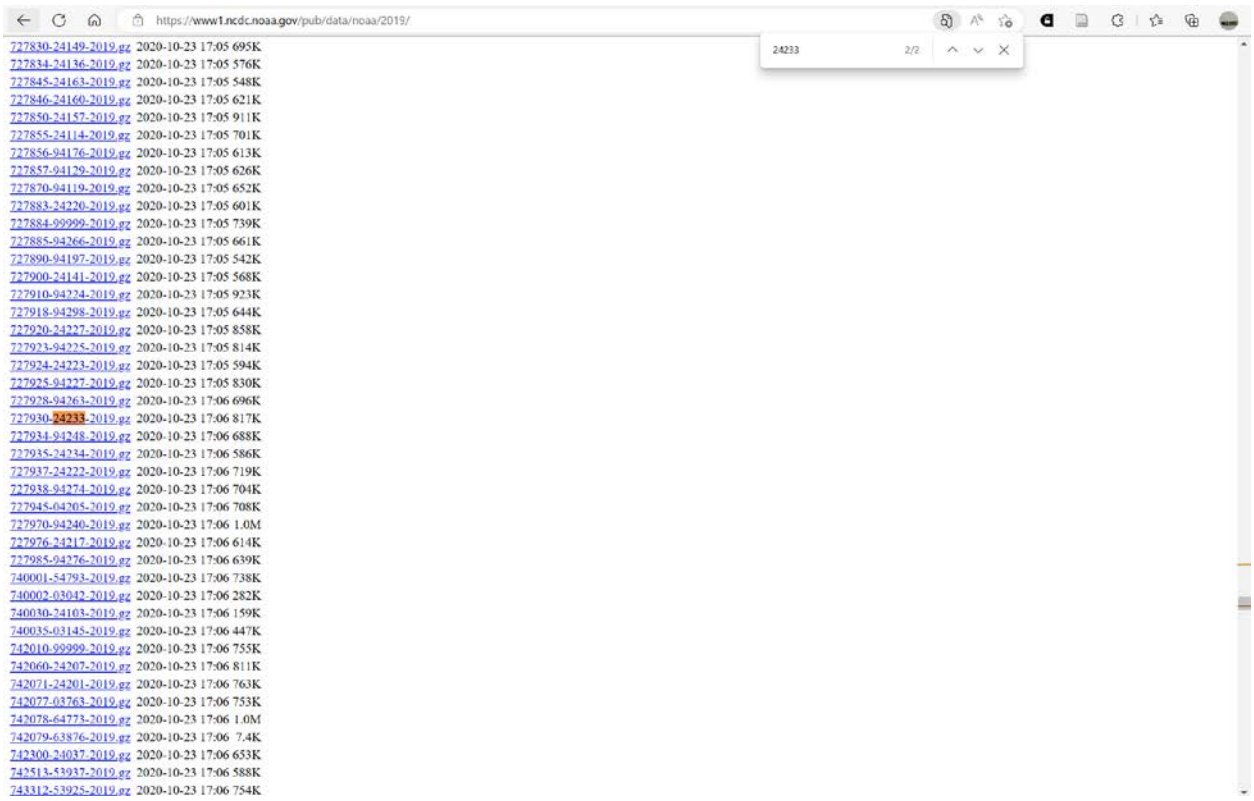
https://www1.ncdc.noaa.gov/pub/data/noaa/2019/
24233
2/2
727830-24149-2019.gz 2020-10-23 17:05 695K
727834-24136-2019.gz 2020-10-23 17:05 576K
727845-24163-2019.gz 2020-10-23 17:05 548K
727846-24160-2019.gz 2020-10-23 17:05 621K
727850-24157-2019.gz 2020-10-23 17:05 911K
727855-24114-2019.gz 2020-10-23 17:05 701K
727856-94176-2019.gz 2020-10-23 17:05 613K
727857-94129-2019.gz 2020-10-23 17:05 626K
727870-94119-2019.gz 2020-10-23 17:05 652K
727883-24220-2019.gz 2020-10-23 17:05 601K
727884-99999-2019.gz 2020-10-23 17:05 739K
727885-94266-2019.gz 2020-10-23 17:05 661K
727890-94197-2019.gz 2020-10-23 17:05 542K
727900-24141-2019.gz 2020-10-23 17:05 568K
727910-94224-2019.gz 2020-10-23 17:05 923K
727918-94298-2019.gz 2020-10-23 17:05 644K
727920-24227-2019.gz 2020-10-23 17:05 858K
727923-94225-2019.gz 2020-10-23 17:05 814K
727924-24223-2019.gz 2020-10-23 17:05 594K
727925-94227-2019.gz 2020-10-23 17:05 830K
727928-94263-2019.gz 2020-10-23 17:06 696K
727930-24233-2019.gz 2020-10-23 17:06 817K
727934-94248-2019.gz 2020-10-23 17:06 688K
727935-24234-2019.gz 2020-10-23 17:06 586K
727937-24222-2019.gz 2020-10-23 17:06 719K
727938-94274-2019.gz 2020-10-23 17:06 704K
727945-64205-2019.gz 2020-10-23 17:06 708K
727970-94240-2019.gz 2020-10-23 17:06 1.0M
727976-24217-2019.gz 2020-10-23 17:06 614K
727985-94276-2019.gz 2020-10-23 17:06 639K
740001-54793-2019.gz 2020-10-23 17:06 738K
740002-03042-2019.gz 2020-10-23 17:06 282K
740030-24103-2019.gz 2020-10-23 17:06 159K
740035-03145-2019.gz 2020-10-23 17:06 447K
742010-99999-2019.gz 2020-10-23 17:06 755K
742060-24207-2019.gz 2020-10-23 17:06 811K
742071-24201-2019.gz 2020-10-23 17:06 763K
742077-03763-2019.gz 2020-10-23 17:06 753K
742078-64773-2019.gz 2020-10-23 17:06 1.0M
742079-63876-2019.gz 2020-10-23 17:06 7.4K
742300-24037-2019.gz 2020-10-23 17:06 653K
742513-53937-2019.gz 2020-10-23 17:06 588K
743312-53925-2019.gz 2020-10-23 17:06 754K

Part A2 Starting AERMET and loading government meteorological data into AERMET

Click on AERMET View icon to start AERMET program (see snapshot of welcome screen). We use AERMET View version 10.2.1 for this thesis.

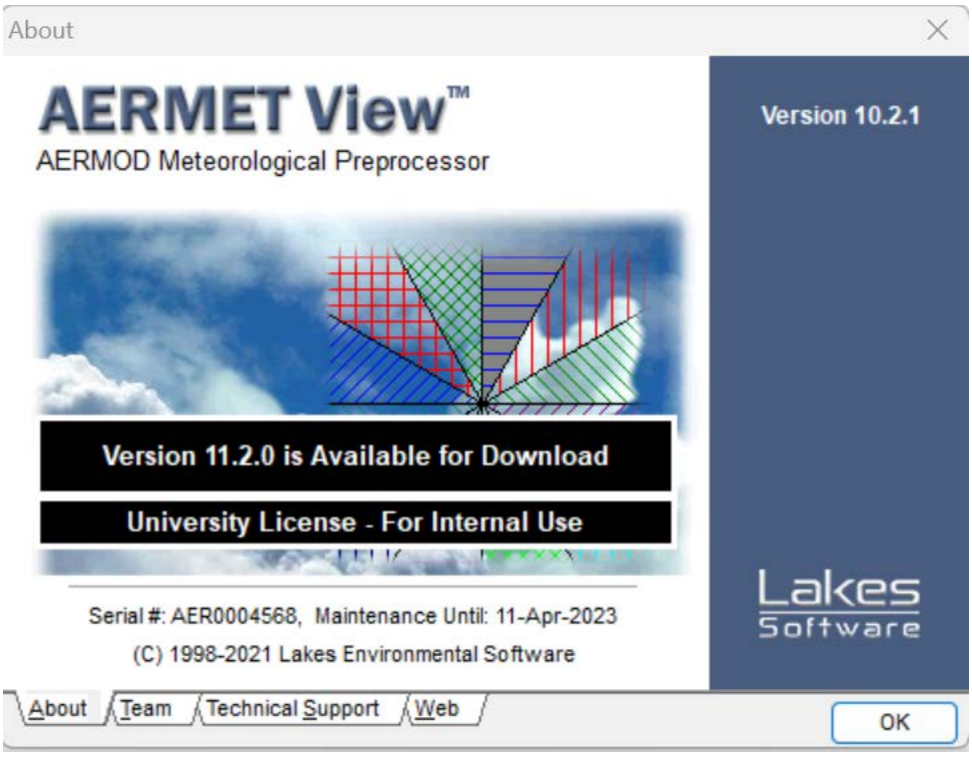

Start new AERMET project file and save it to project folder.

Load Surface atmosphere file: 727930-24233-2019

Remember to load the unzipped file 727930-24233-2019, not 727930-24233-2019.gz

Format is NCDC TD-3505 (ISHD – full archival) because that is the downloaded file format.

If the loading is correct, AERMET will recognize and auto-output Station ID: 24233. Name: SEATTLE-TACOMA INTERNATIONAL AIRPORT. Surface Station Location will also automatically be loaded. (see snapshot below).

Under Data Reported Time, is Surface Data Reported in Local Standard Time (LST)? Answer needs to be "No". The download file 727930-24233-2019 is in TD-3505 format and not in Local Standard Time but in Seattle time. Therefore, adjustment to Local Standard Time is positive 8 hours. (see snapshot above). We know it is positive 8 hours because there is not a negative sign in the selected value.

Now switch to loading upper atmosphere data. Load the file 2019.FSL.txt.

Mode is the default Standard AERMET because we are using download upper atmospheric data, which is real data and not simulated.

Choose FSL for format. Even the file is in .txt, because the spacing of the rows and columns of the data is in FSL.

AERMET should automatically recognize Station ID: 94240. (see snapshot below)

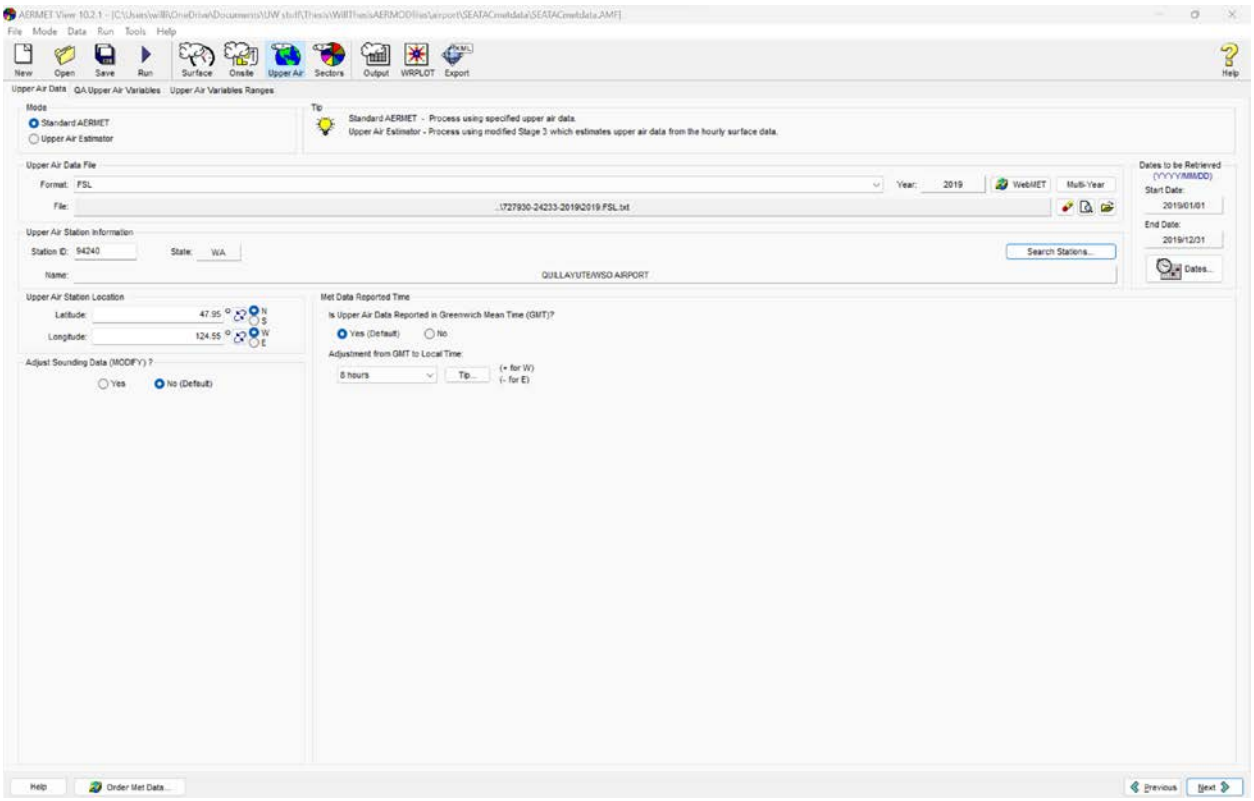

Under Met Data Reported Time, Is Upper Air Data Reported in Greenwich Mean Time (GMT) needs to be Yes.

Adjustment from GMT to Local Time needs to be positive 8 hours. (see snapshot above).

Part A3: AERSURFACE

AERSURFACE is a software within AERMET view embedded by the AERMET button "Sector". The purpose of AERSURFACE is to tell AERMET what kind of land surface is the wind interacting during AERMET intersection.

We are going to use our downloaded files surface parameters by doing the following. We are going to check "Use the File Instead of Sector & Surface Parameter in the AERMET input file". Then we click AERSURFACE. (see snapshot below)

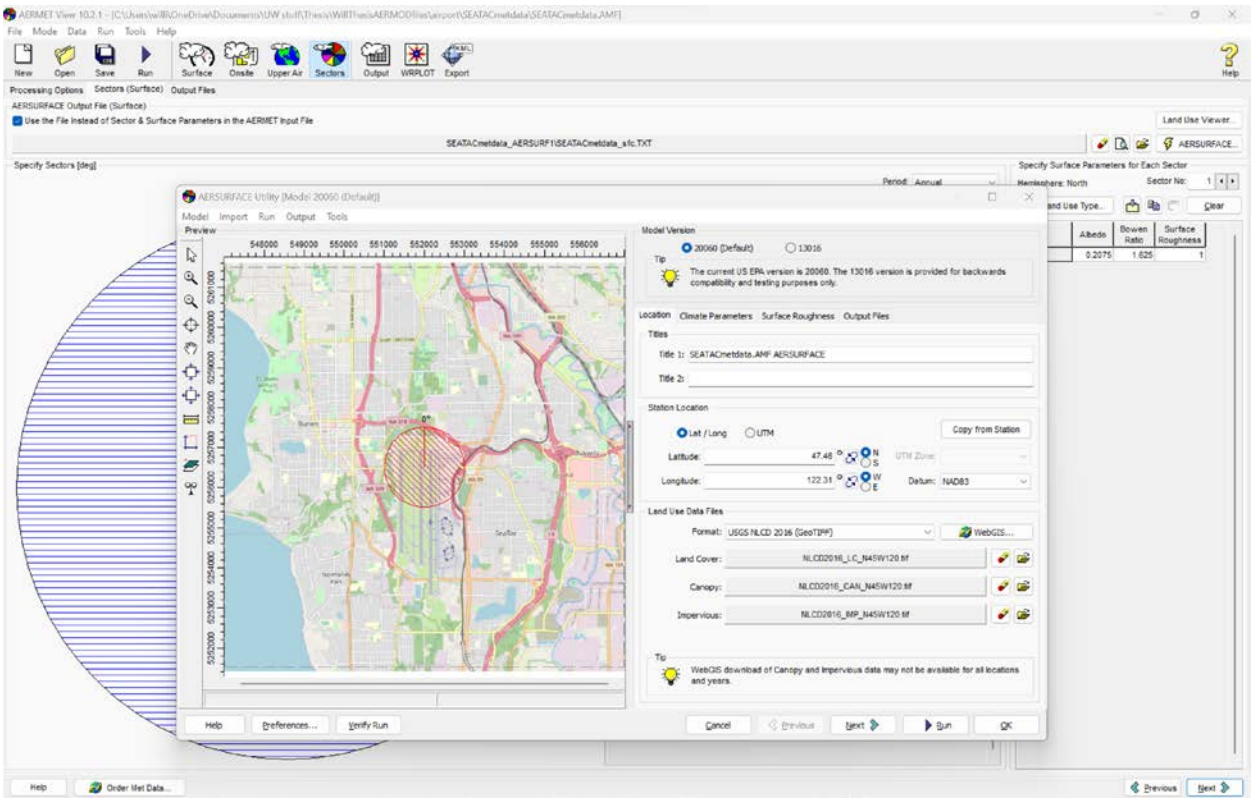

Then we click run to get real surface data. (see snapshot below)

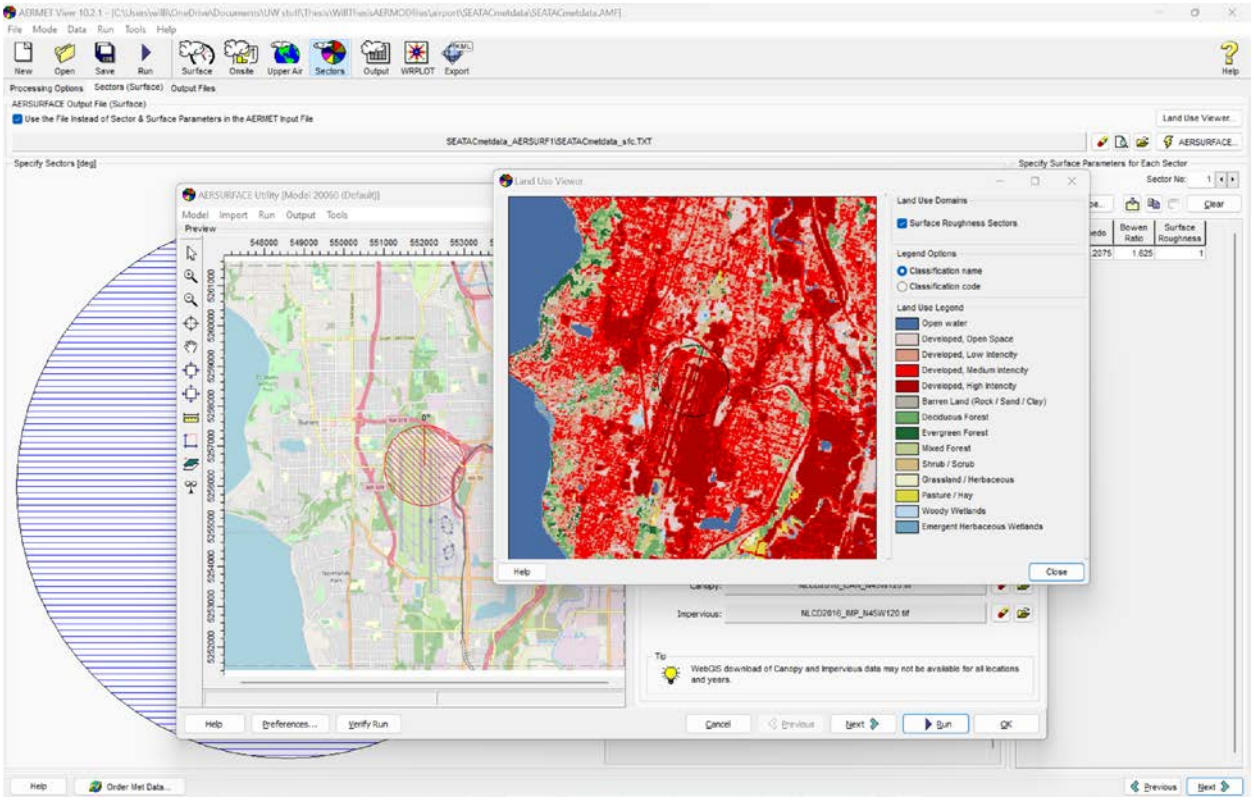

Click close and leave AERSURACE

Part A4: Running AERMET simulation

We are going to click the Run button and the Run screen will show up. (see snapshot below).

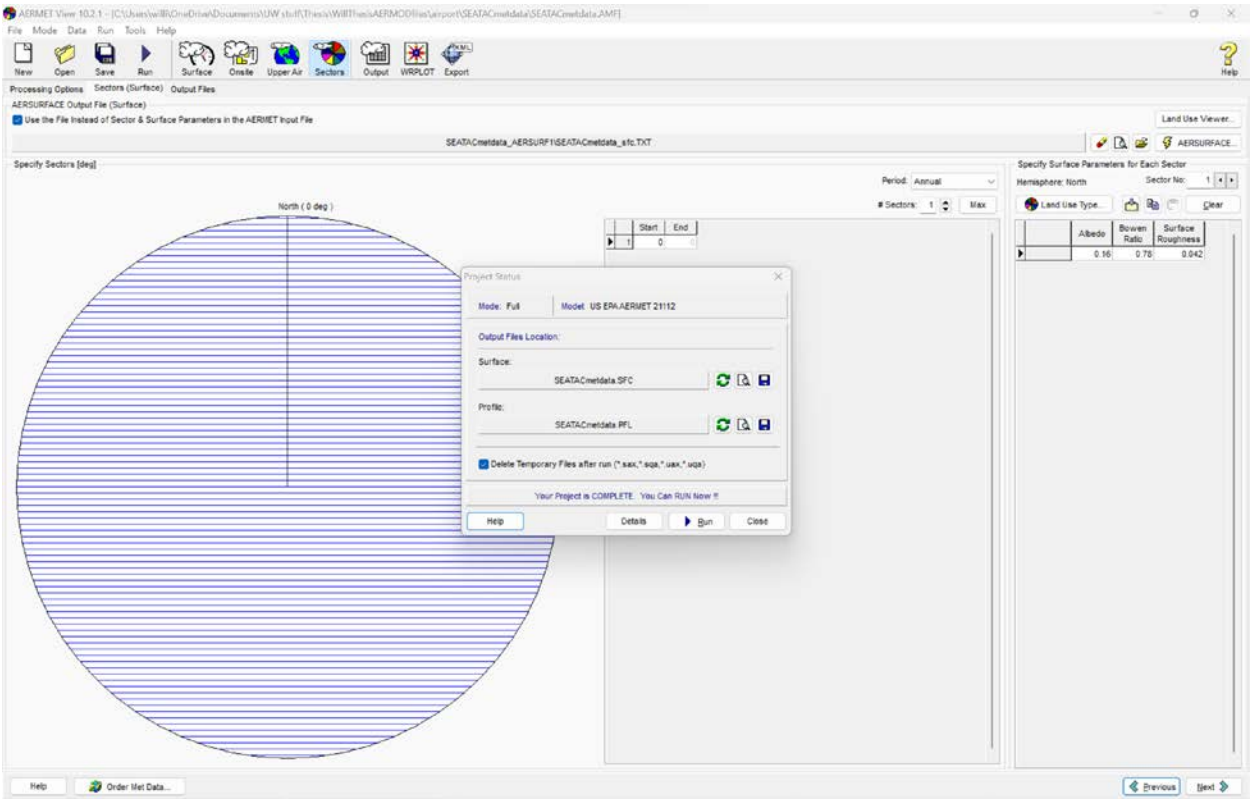

The final desired output is SEATACmetdata.SFC (processed surface file) and SEATACmetdata.PFL (processed profile file).

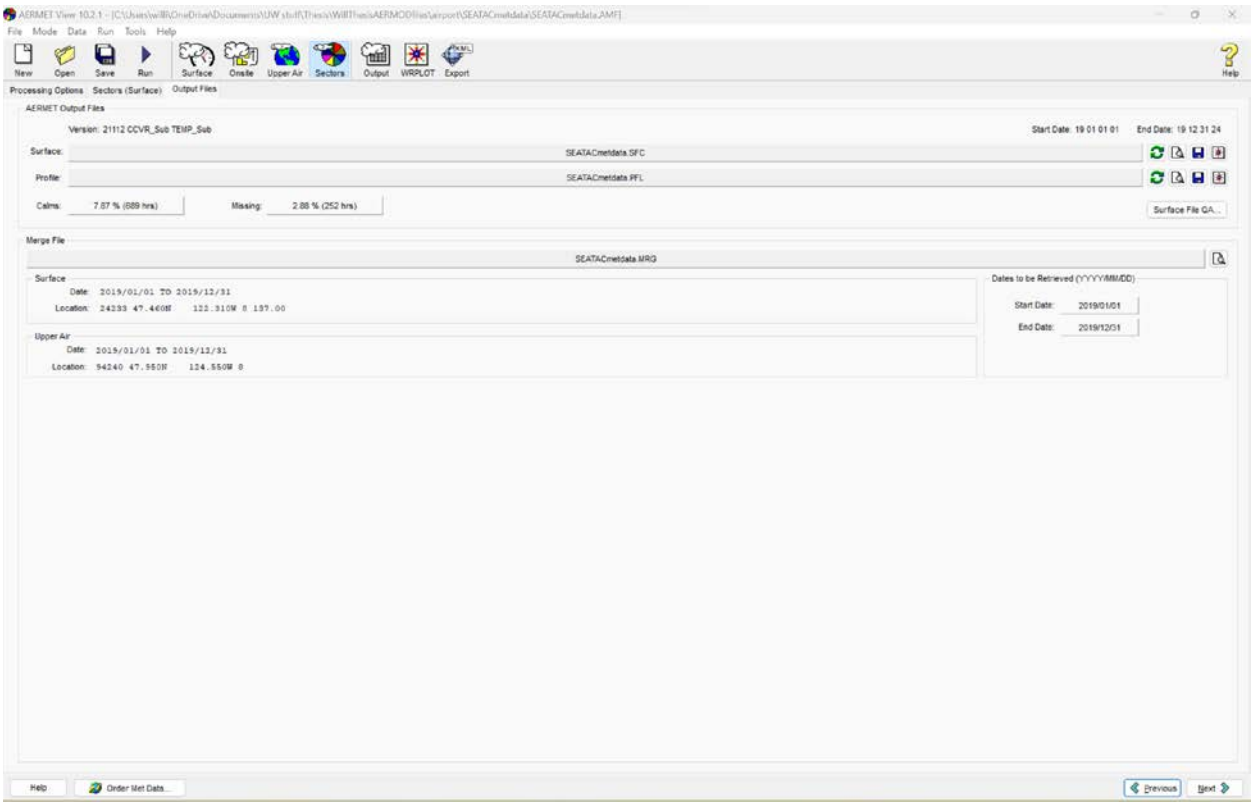

Your work in AERMET is now completed and .SFC and .PFL files are now in your project folder.

Part B1: Starting AERMOD version 10.2.1

There will be 4 independent simulations. Southboundlanding. Southboundtakeoff. Northboundlanding. Northboundtakeoff.

Open AERMOD 10.2.1. Click New. Create New Project. Each project will be a single simulation among one of the 4 simulations.

Under specific new project name and location: type in the project name of your choice. (see snapshot below). Since I have already completed the 4 simulations, my snapshot uses the project name GenericExampleLanding to not cause any confusion for my existing simulation.

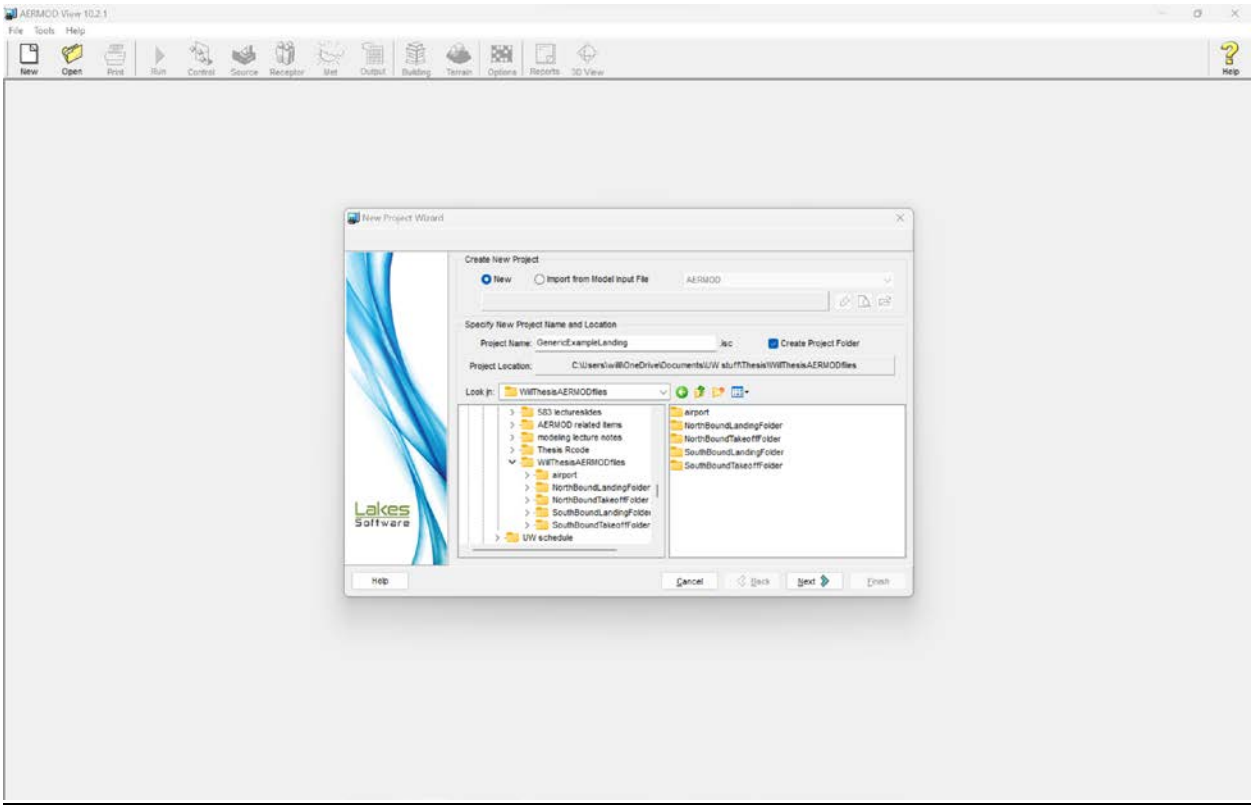

Click next and the software will ask UTM zone. UTM zone is the same for all 4 simulation because the location of SEATAC airport has a single UTM zone = 10. Hemisphere = North. (See snapshot below)

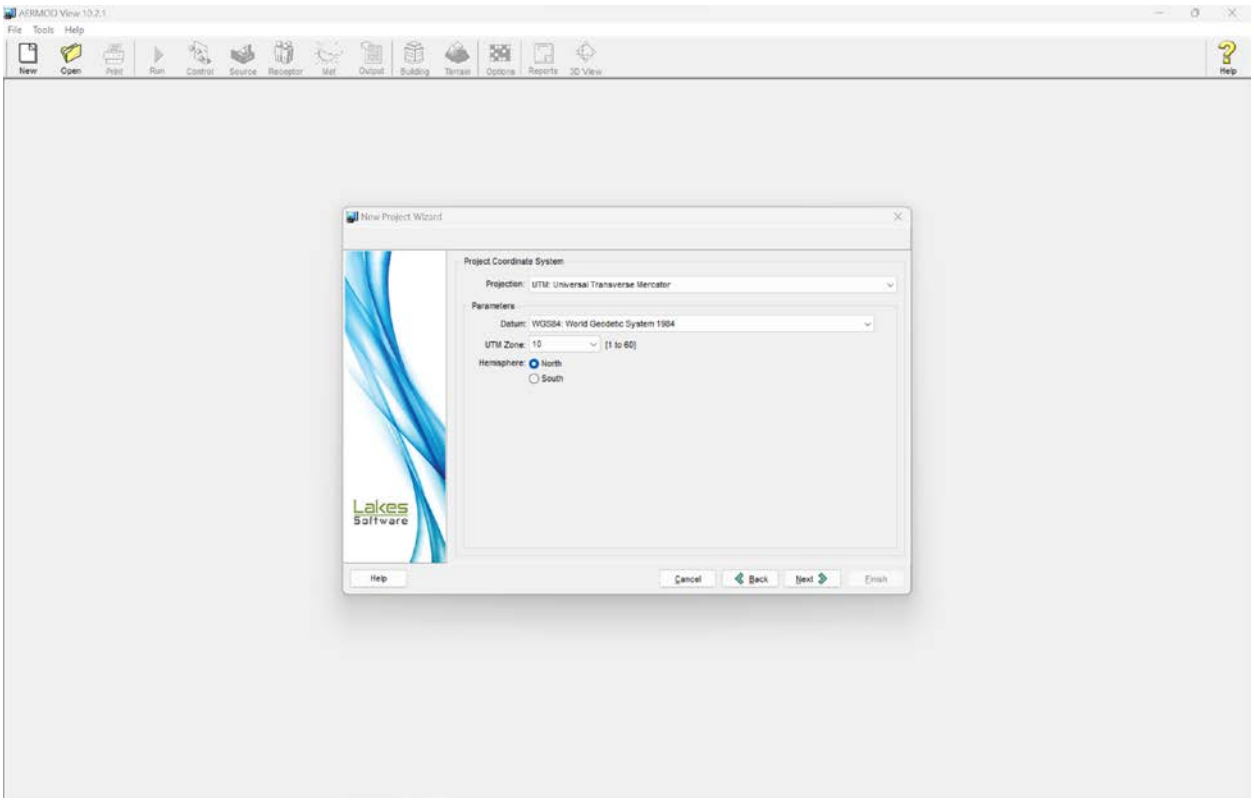

Part B2: Loading SEATAC area map into AERMOD

Click next. Click on Lat/Long to input SEATAC airport coordinates. (See snaphot below)

Lat = 47.4502° N

Long =122.3088° W

Reference point is center because we want our simulation to be centered around SEATAC airport. Radius is 40km because we do not expect air pollution of SEATAC aircraft traffic to have significant impact below 40km. This 40km cutoff is secondary to the landing angle of 4 degrees and boundary layer likely to be below 1000 meters.

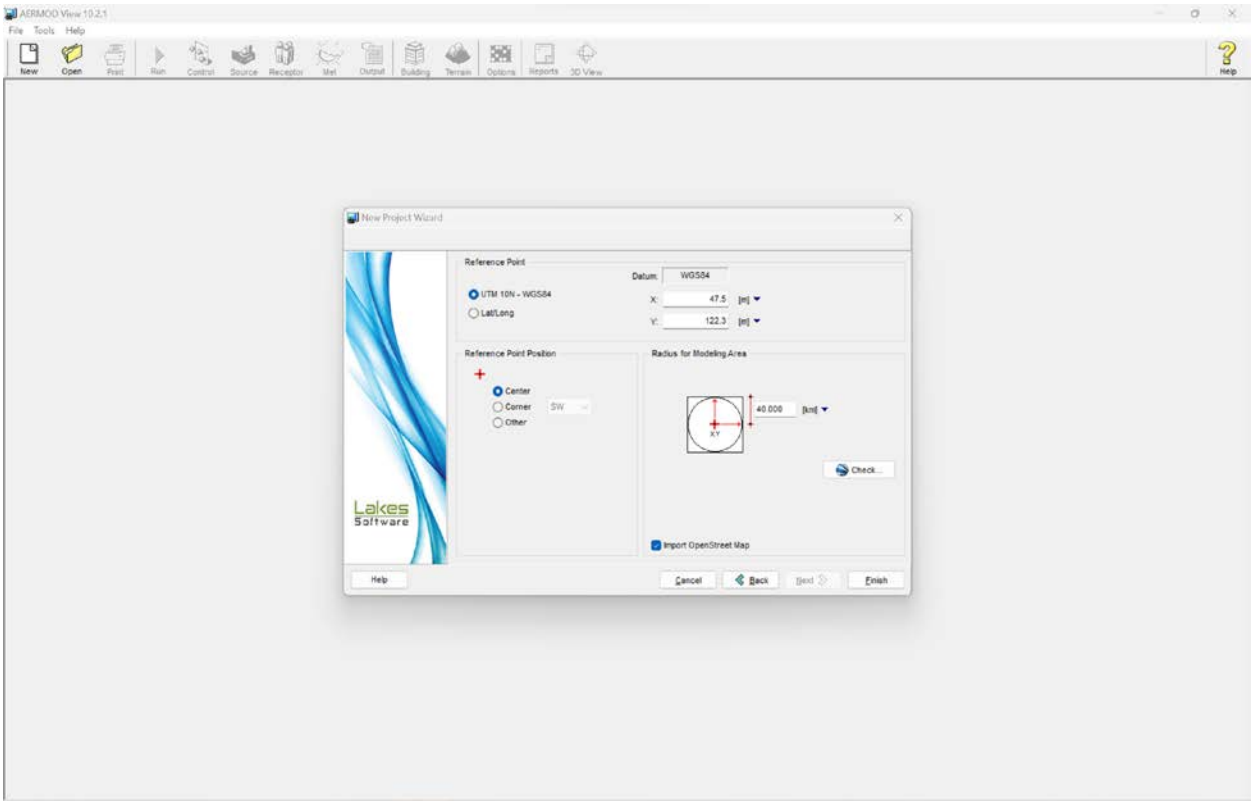

Push finish and you will get a map centered on SEATAC

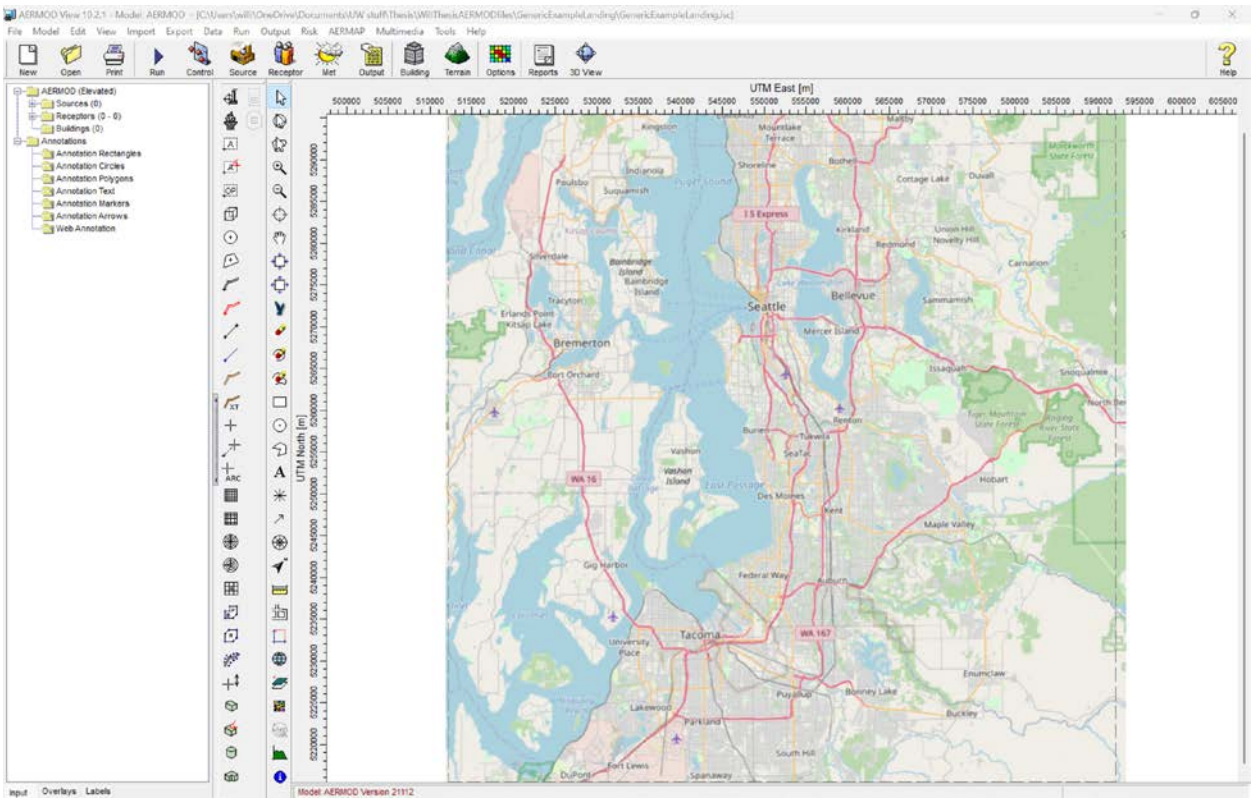

Part B3: Setting Cartesian Grid

Start an Uniform Cartesian Grid Network

Adjust center of the grid to be at the center of runway 3 of SEATAC airport.

Center coordinate X = 551400. Y = 5255536 because that is the center of SEATAC airport runway 3.

Number of points X-axis 21 Y-Axis 83.

Spacing X =1000 and Y =1000.

These setting will result in a rectangular receptor grid with 20km and 82km, centered on runway 3 with the long axis parallel to longitude. This arrangement allows the same grid to be used for both North bound and south bound traffic even only one simulation is run at a time. There are 1743 receptors, and each receptor is a point to record intensity of UFP exposure in the simulation.

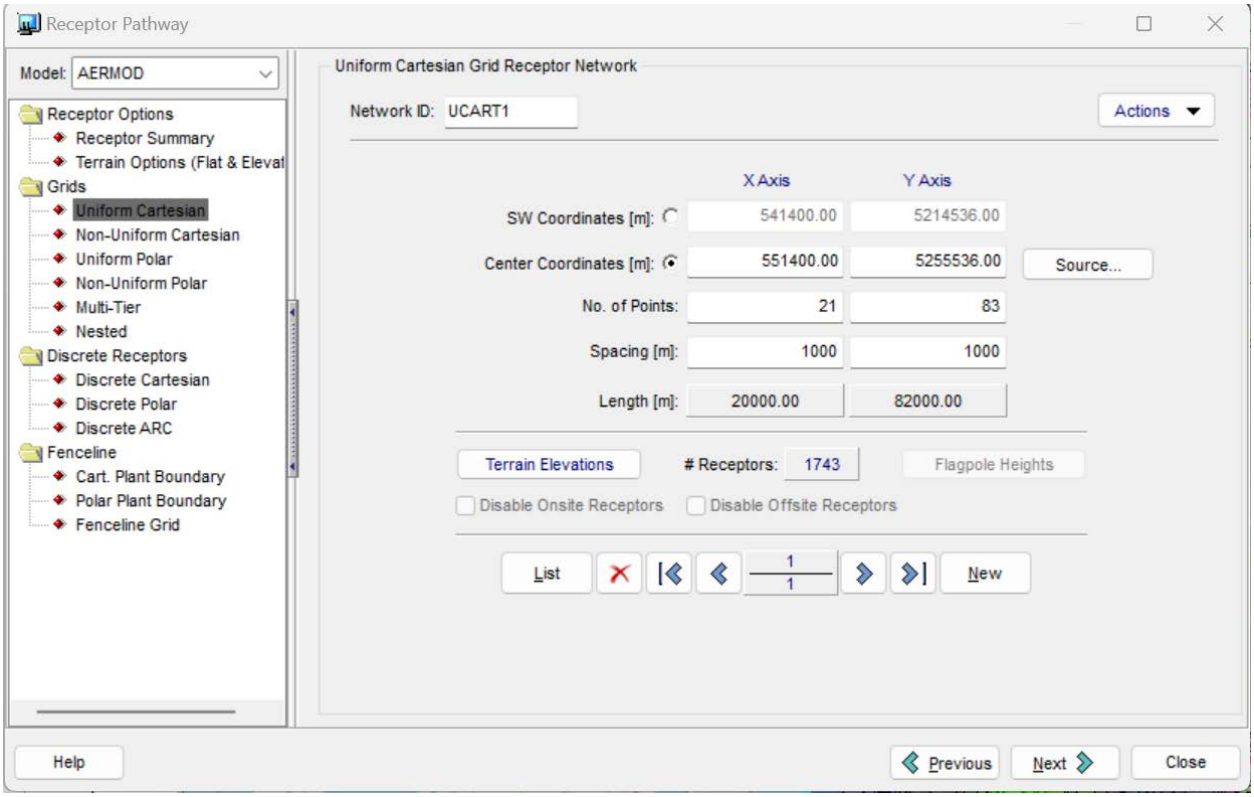

Part B4: Setting Southbound Landing Path Source (see snapshots below)

During this step, we are setting up the southbound landing simulation. Each simulation is different only by its source. There will be one source path per simulation. And here we are setting up the Southbound Landing Path source. We choose the source type to be line volume source. Line volume source is made of a series of boxes that allow air mixing within the box before release.

South Bound Landing Volume Line Source:

Node #1 = X Coord: 551400.00 Y Coord: 5256900.00 Base elevation: 0

Node #2 = X Coord: 551400.00 Y Coord: 5276900.00 Base elevation: 1000

Plume Height: 50m

Plume width: 50m

Emission Rate: 1g/s

Node #1 is touching the northern most tip of runway 3 on the ground. Node #2 is locating 20km north of Node #1 horizontally and 1000 meter elevated. The 1000-meter elevation is chosen to be set above the boundary layer height. Therefore, we expect this source path to cross the

boundary layer. Plume height and wide is 50m x 50m to simulate the wake turbulence generated by the wings and the mixing of air.

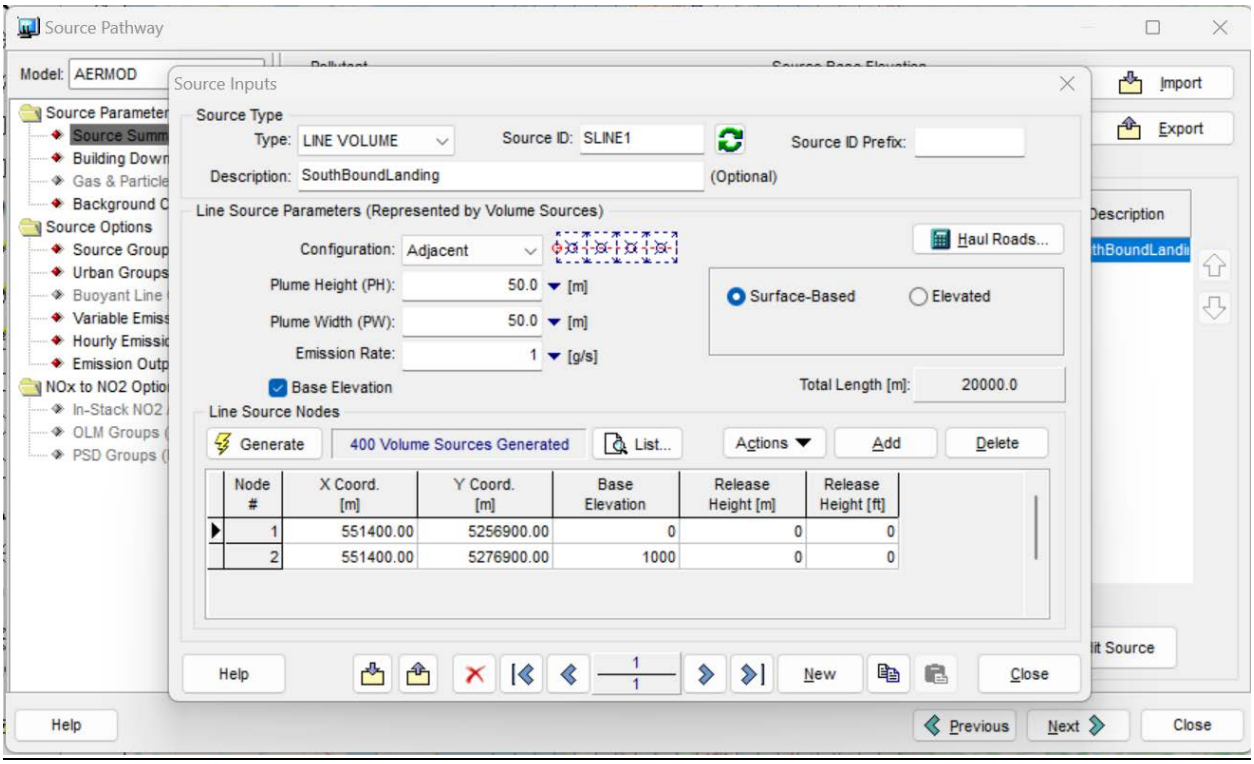

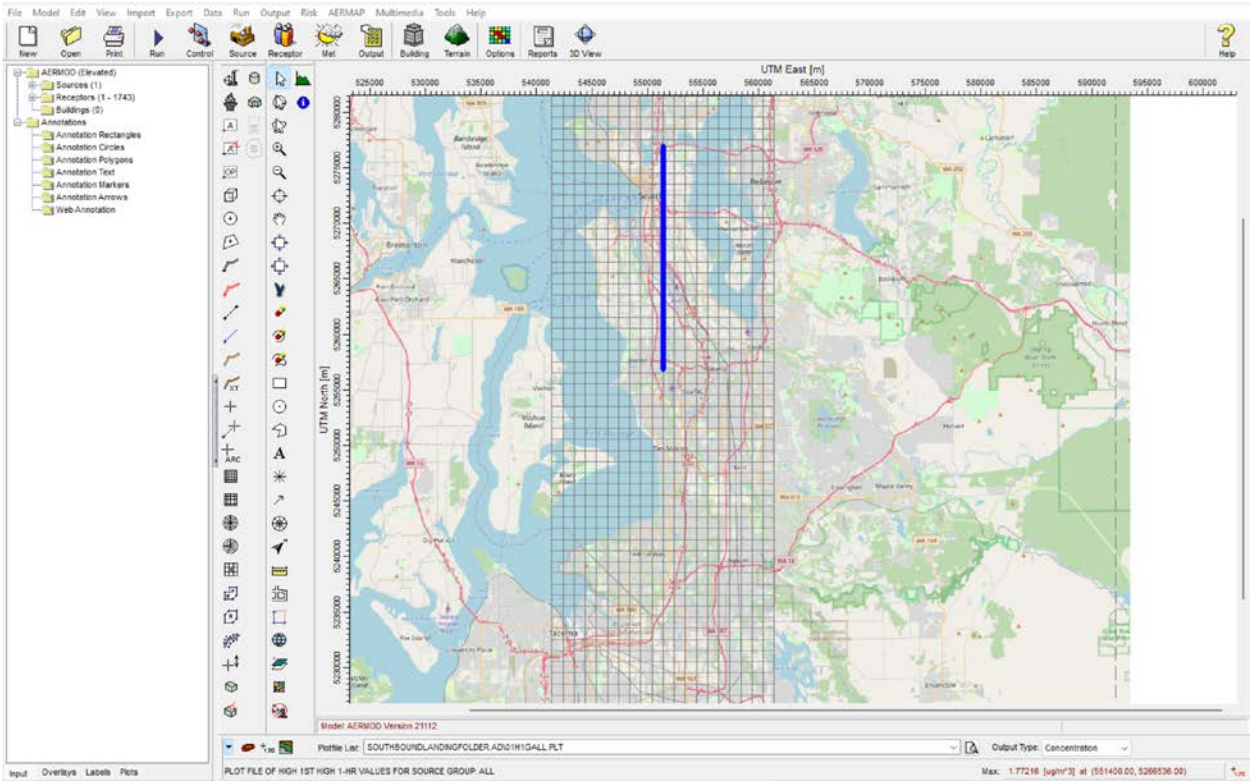

<u>Part B5: load AERMET meterological pathway files (SFC and PFL) into AERMOD (see snapshots below)</u>

Loading meteorological pathway file by click the sun icon. Surface met data file is the SFC file we processed by AERMET. Profile met data file is the PFL file we processed by AERMET. The data range is preset by the SFC file and PFL file. The station number is 24233 is also preset by the SFC file and PFL file. You must load meteorological files before continuing your simulation. Surface station primary met tower (Anemometer) 451.0ft is a preset.

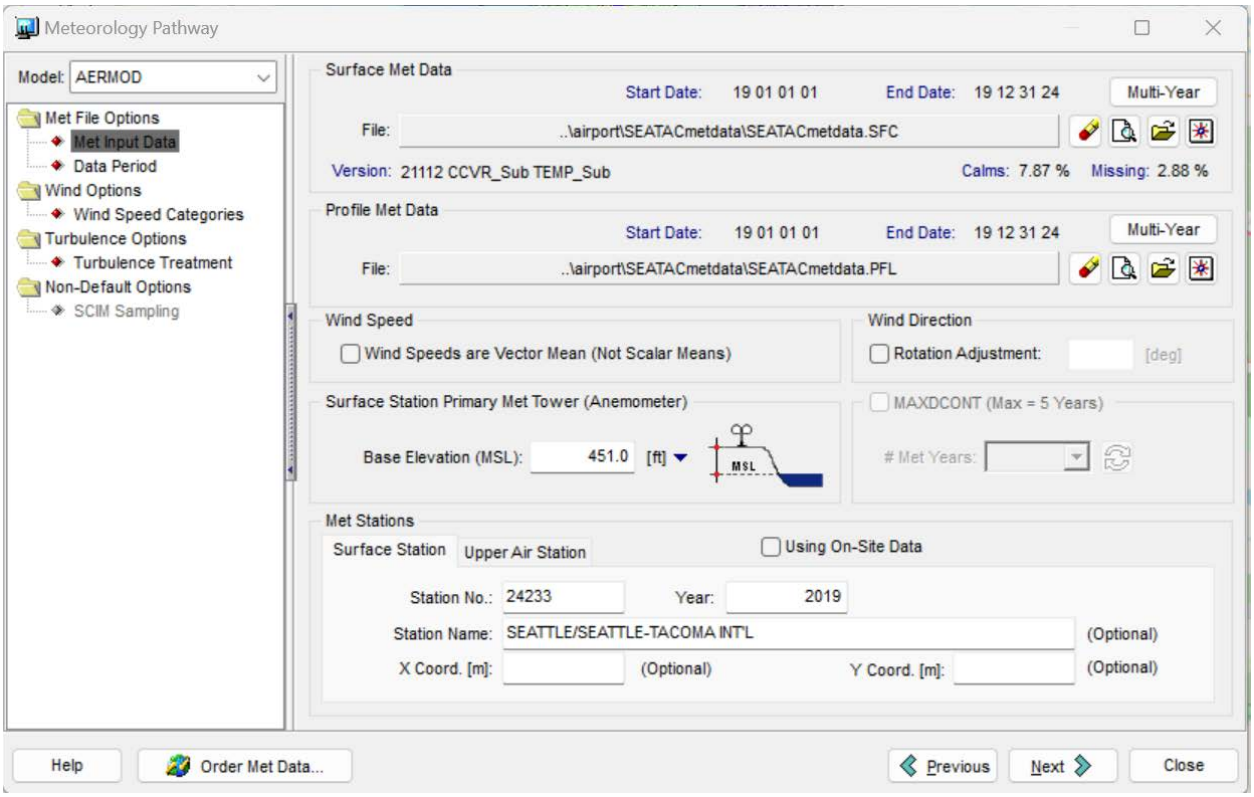

Click data period to choose the days of Southbound traffic.

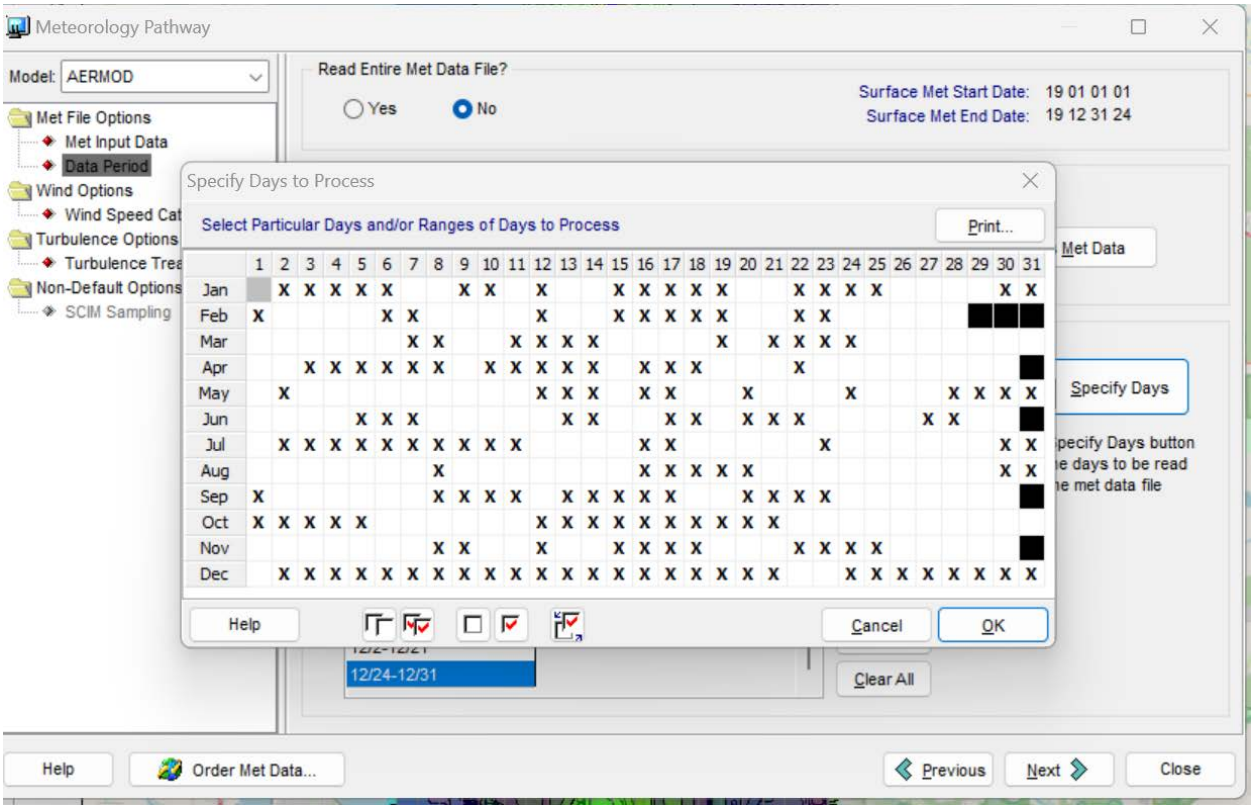

Part B6: load terrain file. See snapshots below (see snapshot below)

The purpose of loading terrain file is terrain can influence UFP pollution distribution. Map type is NED Geotiff. Choose flat and elevated. Push process + run AERMAP to download NED Geotiff map from the internet for your receptor grid.

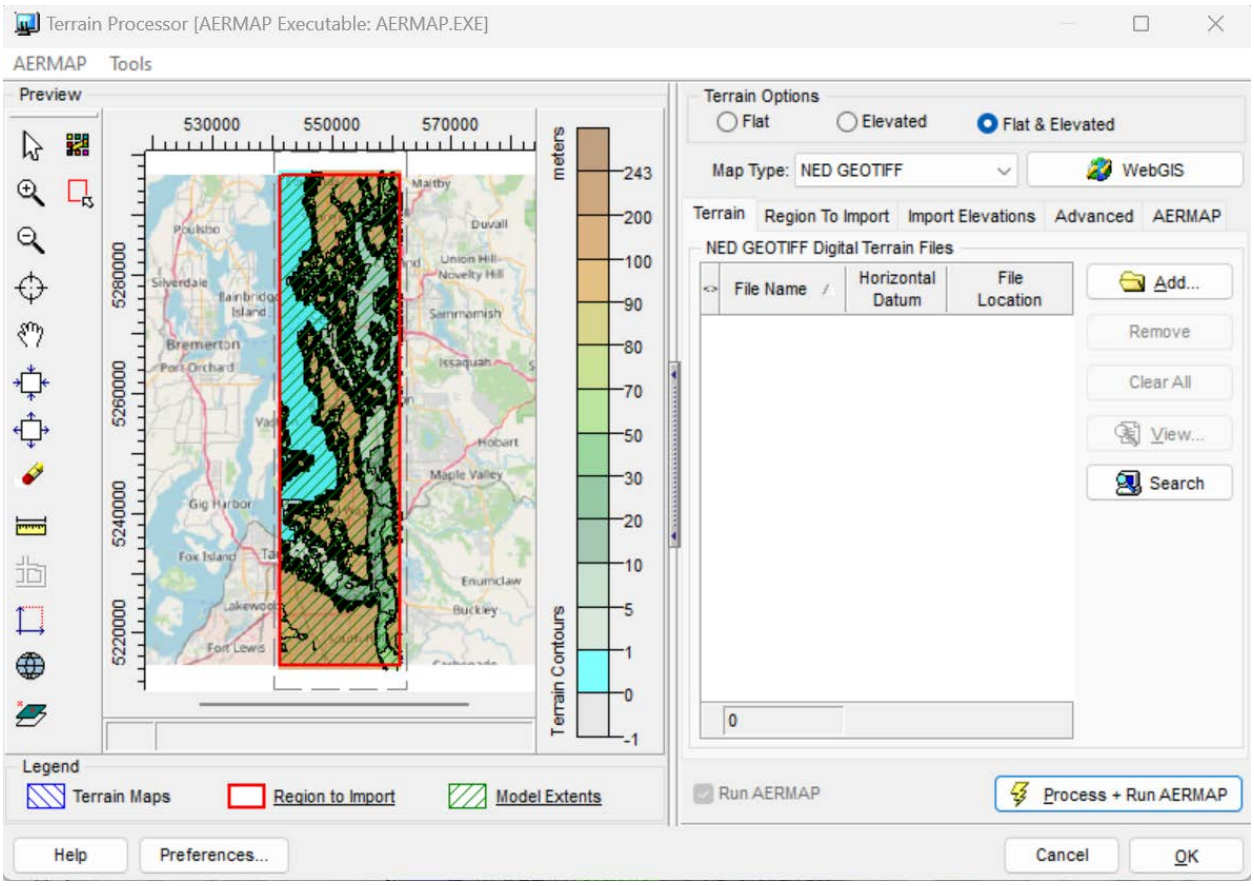

Part C: Run AERMOD (see snapshot below)

After you have load the meteorological data, the terrain data, the receptor grid, and the volume line source, you would have enough setting to run AERMOD. Simply push the run button to run AERMOD.

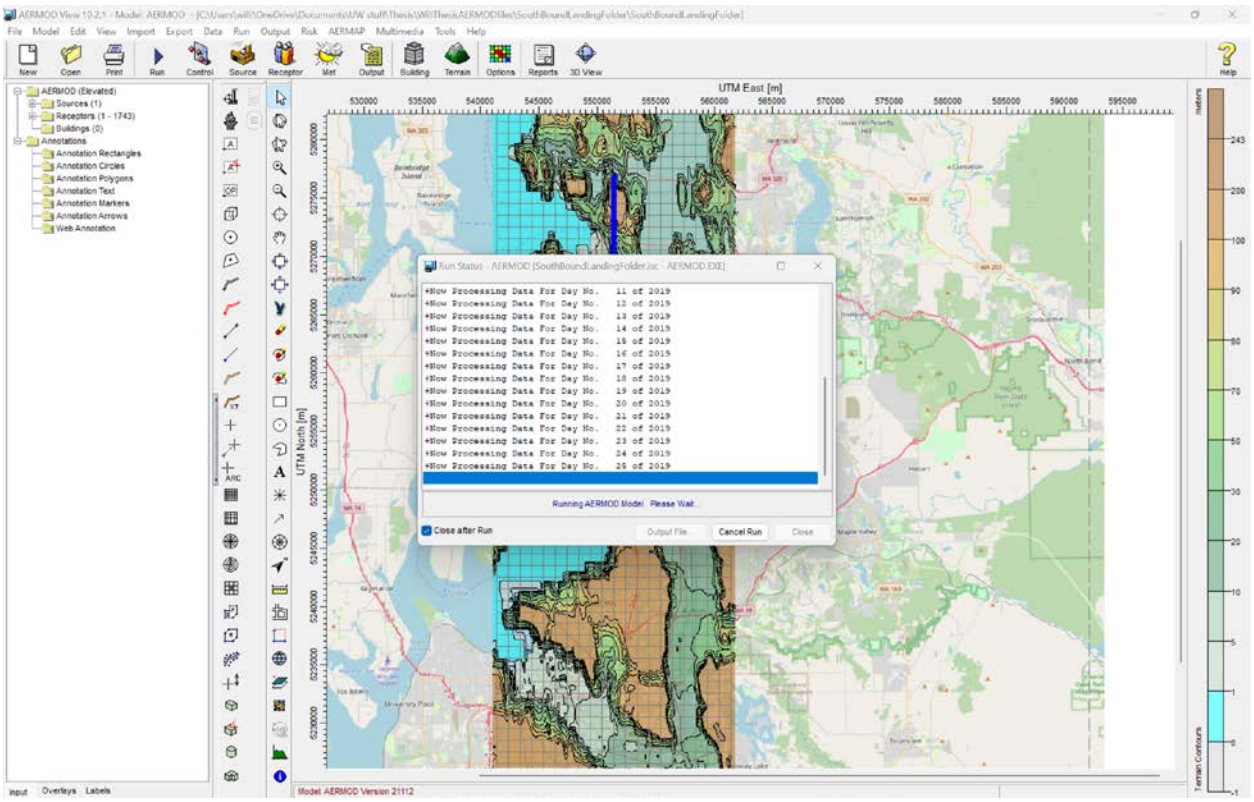

The plan is to repeat the Part C for all four simulation and get Figure 3 to Figure 6.

REFERENCES:

1. Patterson C. World Alzheimer Report 2018: The state of the art of dementia research: New frontiers. Published online September 21, 2018. Accessed October 26, 2022. https://www.alzint.org/resource/world-alzheimer-report-2018/

2. Livingston G, Huntley J, Sommerlad A, et al. Dementia prevention, intervention, and care: 2020 report of the Lancet Commission. *Lancet*. 2020;396(10248):413-446. doi:10.1016/S0140-6736(20)30367-6

3. Selkoe DJ. The molecular pathology of Alzheimer's disease. *Neuron*. 1991;6(4):487-498. doi:10.1016/0896-6273(91)90052-2

4. Serrano-Pozo A, Frosch MP, Masliah E, Hyman BT. Neuropathological alterations in Alzheimer disease. *Cold Spring Harb Perspect Med*. 2011;1(1):a006189. doi:10.1101/cshperspect.a006189

5. Braak H, Braak E. Neuropathological stageing of Alzheimer-related changes. *Acta Neuropathol*. 1991;82(4):239-259. doi:10.1007/BF00308809

6. Calderón-Garcidueñas L, Ayala A. Air Pollution, Ultrafine Particles, and Your Brain: Are Combustion Nanoparticle Emissions and Engineered Nanoparticles Causing Preventable Fatal Neurodegenerative Diseases and Common Neuropsychiatric Outcomes? *Environ Sci Technol*. 2022;56(11):6847-6856. doi:10.1021/acs.est.1c04706

7. Power MC, Adar SD, Yanosky JD, Weuve J. Exposure to air pollution as a potential contributor to cognitive function, cognitive decline, brain imaging, and dementia: A systematic review of epidemiologic research. *Neurotoxicology*. 2016;56:235-253. doi:10.1016/j.neuro.2016.06.004

8. Oudin A, Forsberg B, Nordin Adolfsson A, Lind N, Modig L, Nordin M, Nordin S, Adolfsson R, Nilsson LG. 2016. Traffic-related air pollution and dementia incidence in northern Sweden: a longitudinal study. Environ Health Perspect 124:306–312; http://dx.doi.org.offcampus.lib.washington.edu/10.1289/ehp.1408322

9. Chen H, Kwong JC, Copes R, et al. Living near major roads and the incidence of dementia, Parkinson's disease, and multiple sclerosis: a population-based cohort study. *Lancet*. 2017;389(10070):718-726. doi:10.1016/S0140-6736(16)32399-6

10. Yuchi W, Sbihi H, Davies H, Tamburic L, Brauer M. Road proximity, air pollution, noise, green space and neurologic disease incidence: a population-based cohort study. *Environ Health*. 2020;19(1):8. doi:10.1186/s12940-020-0565-4

11. Calderón-Garcidueñas L, Reed W, Maronpot RR, et al. Brain inflammation and Alzheimer's-like pathology in individuals exposed to severe air pollution. *Toxicol Pathol*. 2004;32(6):650-658. doi:10.1080/01926230490520232

12. Calderón-Garcidueñas L, Solt AC, Henríquez-Roldán C, et al. Long-term air pollution exposure is associated with neuroinflammation, an altered innate immune response, disruption of the blood-brain barrier, ultrafine particulate deposition, and accumulation of amyloid beta-42 and alpha-synuclein in children and young adults. *Toxicol Pathol*. 2008;36(2):289-310. doi:10.1177/0192623307313011

13. Calderón-Garcidueñas L, Franco-Lira M, Henríquez-Roldán C, et al. Urban air pollution: influences on olfactory function and pathology in exposed children and young adults. *Exp Toxicol Pathol*. 2010;62(1):91-102. doi:10.1016/j.etp.2009.02.117

14. Calderón-Garcidueñas L, Mora-Tiscareño A, Ontiveros E, et al. Air pollution, cognitive deficits and brain abnormalities: a pilot study with children and dogs. *Brain Cogn*. 2008;68(2):117-127. doi:10.1016/j.bandc.2008.04.008

15. Durga M, Devasena T, Rajasekar A. Determination of LC50 and sub-chronic neurotoxicity of diesel exhaust nanoparticles. *Environ Toxicol Pharmacol*. 2015;40(2):615-625. doi:10.1016/j.etap.2015.06.024

16. Bhatt DP, Puig KL, Gorr MW, Wold LE, Combs CK. A pilot study to assess effects of long-term inhalation of airborne particulate matter on early Alzheimer-like changes in the mouse brain. *PLoS One*. 2015;10(5):e0127102. doi:10.1371/journal.pone.0127102

17. Kim SH, Knight EM, Saunders EL, et al. Rapid doubling of Alzheimer's amyloid-β40 and 42 levels in brains of mice exposed to a nickel nanoparticle model of air pollution. *F1000Res*. 2012;1:70. doi:10.12688/f1000research.1-70.v1

18. Block ML, Calderón-Garcidueñas L. Air pollution: mechanisms of neuroinflammation and CNS disease. *Trends Neurosci*. 2009;32(9):506-516. doi:10.1016/j.tins.2009.05.009

19. Jayaraj RL, Rodriguez EA, Wang Y, Block ML (2017) Outdoor Ambient Air Pollution and Neurodegenerative Diseases: the Neuroinflammation Hypothesis. Curr Environ Health Rep 4, 166–179. [PubMed: 28444645]

20. Heusinkveld HJ, Wahle T, Campbell A, Westerink RHS, Tran L, Johnston H, Stone V, Cassee FR, Schins RPF (2016) Neurodegenerative and neurological disorders by small inhaled particles. Neurotoxicology 56, 94–106. [PubMed: 27448464]

21. Shaffer RM, Li G, Adar SD, et al. Fine Particulate Matter and Markers of Alzheimer's Disease Neuropathology at Autopsy in a Community-Based Cohort. *JAD*. 2021;79(4):1761-1773. doi:10.3233/JAD-201005

22. Galasko D, Montine TJ. Biomarkers of oxidative damage and inflammation in Alzheimer's disease. *Biomark Med*. 2010;4(1):27-36. doi:10.2217/bmm.09.89

23. Golden TR, Hinerfeld DA, Melov S (2002) Oxidative stress and aging: beyond correlation. Aging Cell 1, 117–123.

24. Kukull WA, Higdon R, Bowen JD, et al. Dementia and Alzheimer disease incidence: a prospective cohort study. *Arch Neurol*. 2002;59(11):1737-1746. doi:10.1001/archneur.59.11.1737

25. Policy | Federal Aviation Administration. Accessed February 6, 2023. https://www.faa.gov/about/office_org/headquarters_offices/apl/environ_policy_guidance/policy/faa_nepa_order

26. Aviation Environmental Tools Suite | Federal Aviation Administration. Accessed February 6, 2023. https://www.faa.gov/about/office_org/headquarters_offices/apl/aee/research/models

27. Sonnen JA, Larson EB, Crane PK, et al. Pathological correlates of dementia in a longitudinal, population-based sample of aging. *Ann Neurol*. 2007;62(4):406-413. doi:10.1002/ana.21208

28. Bennett DA, Schneider JA, Arvanitakis Z, et al. Neuropathology of older persons without cognitive impairment from two community-based studies. *Neurology*. 2006;66(12):1837-1844. doi:10.1212/01.wnl.0000219668.47116.e6

29. Variable Details | RADC. Accessed October 23, 2022. https://www.radc.rush.edu/docs/var/detail.htm?category=Pathology&subcategory=Alzheimer%27s+disease&variable=ceradsc

30. Koychev I, Hofer M, Friedman N. Correlation of Alzheimer Disease Neuropathologic Staging with Amyloid and Tau Scintigraphic Imaging Biomarkers. *J Nucl Med*. 2020;61(10):1413-1418. doi:10.2967/jnumed.119.230458

31. Murayama S, Saito Y. Neuropathological diagnostic criteria for Alzheimer's disease. *Neuropathology*. 2004;24(3):254-260. doi:10.1111/j.1440-1789.2004.00571.x

32. Blanco MN, Gassett A, Gould T, et al. Characterization of Annual Average Traffic-Related Air Pollution Concentrations in the Greater Seattle Area from a Year-Long Mobile Monitoring Campaign. *Environ Sci Technol*. 2022;56(16):11460-11472. doi:10.1021/acs.est.2c01077

33. Labidi A. Why Airplanes takeoff and land into the wind ? Published online November 21, 2019.

34. Cole SR, Hernán MA. Constructing Inverse Probability Weights for Marginal Structural Models. *Am J Epidemiol*. 2008;168(6):656-664. doi:10.1093/aje/kwn164

35. Hernán MA, Hernández-Díaz S, Robins JM. A Structural Approach to Selection Bias. *Epidemiology*. 2004;15(5):615-625.

36. Hernan MA RJ (2020) Causal Inference: What If., Chapman & Hall/CRC, Boca Raton.

37. Ghebremedhin E, Schultz C, Thal DR, et al. Gender and age modify the association between APOE and AD-related neuropathology. *Neurology*. 2001;56(12):1696-1701. doi:10.1212/wnl.56.12.1696

38. Barnes LL, Wilson RS, Bienias JL, Schneider JA, Evans DA, Bennett DA. Sex Differences in the Clinical Manifestations of Alzheimer Disease Pathology. *Archives of General Psychiatry*. 2005;62(6):685-691. doi:10.1001/archpsyc.62.6.685

39. Clougherty JE. A Growing Role for Gender Analysis in Air Pollution Epidemiology. *Environ Health Perspect*. 2010;118(2):167-176. doi:10.1289/ehp.0900994

40. O'Neill MS, Jerrett M, Kawachi I, et al. Health, wealth, and air pollution: advancing theory and methods. *Environ Health Perspect*. 2003;111(16):1861-1870.

41. Koepsell TD, Kurland BF, Harel O, Johnson EA, Zhou XH, Kukull WA. Education, cognitive function, and severity of neuropathology in Alzheimer disease. *Neurology*. 2008;70(19 Pt 2):1732-1739. doi:10.1212/01.wnl.0000284603.85621.aa

42. Hajat A, Diez-Roux AV, Adar SD, et al. Air Pollution and Individual and Neighborhood Socioeconomic Status: Evidence from the Multi-Ethnic Study of Atherosclerosis (MESA). *Environ Health Perspect*. 2013;121(11-12):1325-1333. doi:10.1289/ehp.1206337

43. Perlin SA, Wong D, Sexton K. Residential proximity to industrial sources of air pollution: interrelationships among race, poverty, and age. *J Air Waste Manag Assoc*. 2001;51(3):406-421. doi:10.1080/10473289.2001.10464271

44. Jones MR, Diez-Roux AV, Hajat A, et al. Race/Ethnicity, Residential Segregation, and Exposure to Ambient Air Pollution: The Multi-Ethnic Study of Atherosclerosis (MESA). *Am J Public Health*. 2014;104(11):2130-2137. doi:10.2105/AJPH.2014.302135

45. Schlesinger D, Grinberg LT, Alba JG, et al. African ancestry protects against Alzheimer's disease-related neuropathology. *Mol Psychiatry*. 2013;18(1):79-85. doi:10.1038/mp.2011.136

46. Court JA, Johnson M, Religa D, et al. Attenuation of Aβ deposition in the entorhinal cortex of normal elderly individuals associated with tobacco smoking. *Neuropathology and Applied Neurobiology*. 2005;31(5):522-535. doi:10.1111/j.1365-2990.2005.00674.x

47. Moreno-Gonzalez I, Estrada LD, Sanchez-Mejias E, Soto C (2013) Smoking exacerbates amyloid pathology in a mouse model of Alzheimer's disease. Nat Commun 4, 1–10.

48. Rovio S, Kåreholt I, Helkala EL, et al. Leisure-time physical activity at midlife and the risk of dementia and Alzheimer's disease. *The Lancet Neurology*. 2005;4(11):705-711. doi:10.1016/S1474-4422(05)70198-8

49. Blondell SJ, Hammersley-Mather R, Veerman JL. Does physical activity prevent cognitive decline and dementia?: A systematic review and meta-analysis of longitudinal studies. *BMC Public Health*. 2014;14:510. doi:10.1186/1471-2458-14-510

50. Buchman AS, Schneider JA, Wilson RS, Bienias JL, Bennett DA. Body mass index in older persons is associated with Alzheimer disease pathology. *Neurology*. 2006;67(11):1949-1954. doi:10.1212/01.wnl.0000247046.90574.0f

51. Hsu DC, Mormino EC, Schultz AP, et al. Lower late-life body-mass index is associated with higher cortical amyloid burden in clinically normal elderly. *J Alzheimers Dis*. 2016;53(3):1097-1105. doi:10.3233/JAD-150987

52. Gu Y, Scarmeas N, Cosentino S, et al. Change in body mass index before and after Alzheimer's disease onset. *Curr Alzheimer Res*. 2014;11(4):349-356.

53. Matsuzaki T, Sasaki K, Tanizaki Y, et al. Insulin resistance is associated with the pathology of Alzheimer disease: the Hisayama study. *Neurology*. 2010;75(9):764-770. doi:10.1212/WNL.0b013e3181eee25f

54. Pruzin JJ, Nelson PT, Abner EL, Arvanitakis Z. Relationship of Type 2 Diabetes to Human Brain Pathology. *Neuropathol Appl Neurobiol*. 2018;44(4):347-362. doi:10.1111/nan.12476

55. Beeri MS, Silverman JM, Davis KL, et al. Type 2 Diabetes Is Negatively Associated With Alzheimer's Disease Neuropathology. *J Gerontol A Biol Sci Med Sci*. 2005;60(4):471-475.

56. Rajagopalan S, Brook RD. Air Pollution and Type 2 Diabetes. *Diabetes*. 2012;61(12):3037-3045. doi:10.2337/db12-0190

57. Auchincloss AH, Diez Roux AV, Dvonch JT, et al. Associations between Recent Exposure to Ambient Fine Particulate Matter and Blood Pressure in the Multi-Ethnic Study of Atherosclerosis (MESA). *Environ Health Perspect*. 2008;116(4):486-491. doi:10.1289/ehp.10899

58. Chen H, Burnett RT, Kwong JC, et al. Spatial association between ambient fine particulate matter and incident hypertension. *Circulation*. 2014;129(5):562-569. doi:10.1161/CIRCULATIONAHA.113.003532

59. Petrovitch H, White LR, Izmirilian G, et al. Midlife blood pressure and neuritic plaques, neurofibrillary tangles, and brain weight at death: the HAAS. Honolulu-Asia aging Study. *Neurobiol Aging*. 2000;21(1):57-62. doi:10.1016/s0197-4580(00)00106-8

60. Beeri MS, Rapp M, Silverman JM, et al. Coronary artery disease is associated with Alzheimer disease neuropathology in APOE4 carriers. *Neurology*. 2006;66(9):1399-1404. doi:10.1212/01.wnl.0000210447.19748.0b

61. Beach TG, Wilson JR, Sue LI, et al. Circle of Willis atherosclerosis: association with Alzheimer's disease, neuritic plaques and neurofibrillary tangles. *Acta Neuropathol*. 2007;113(1):13-21. doi:10.1007/s00401-006-0136-y

62. Zlokovic BV. Neurovascular pathways to neurodegeneration in Alzheimer's disease and other disorders. *Nat Rev Neurosci*. 2011;12(12):723-738. doi:10.1038/nrn3114

63. Braak H, Thal DR, Ghebremedhin E, Del Tredici K. Stages of the Pathologic Process in Alzheimer Disease: Age Categories From 1 to 100 Years. *Journal of Neuropathology & Experimental Neurology*. 2011;70(11):960-969. doi:10.1097/NEN.0b013e318232a379

64. Herr D, Jew K, Wong C, et al. Effects of concentrated ambient ultrafine particulate matter on hallmarks of Alzheimer's disease in the 3xTgAD mouse model. *Neurotoxicology*. 2021;84:172-183. doi:10.1016/j.neuro.2021.03.010

65. Jang S, Kim EW, Zhang Y, et al. Particulate matter increases beta-amyloid and activated glial cells in hippocampal tissues of transgenic Alzheimer's mouse: Involvement of PARP-1. *Biochemical and Biophysical Research Communications*. 2018;500(2):333-338. doi:10.1016/j.bbrc.2018.04.068

66. Cacciottolo M, Morgan TE, Saffari AA, et al. Traffic-related air pollutants (TRAP-PM) promote neuronal amyloidogenesis through oxidative damage to lipid rafts. *Free Radic Biol Med*. 2020;147:242-251. doi:10.1016/j.freeradbiomed.2019.12.023

67. Gilmore-Bykovskyi AL, Jin Y, Gleason C, et al. Recruitment and retention of underrepresented populations in Alzheimer's disease research: A systematic review. *Alzheimers Dement (N Y)*. 2019;5:751-770. doi:10.1016/j.trci.2019.09.018

68. Crane PK, Walker R, Hubbard RA, et al. Glucose Levels and Risk of Dementia. *N Engl J Med*. 2013;369(6):540-548. doi:10.1056/NEJMoa1215740

69. Austin E, Xiang J, Gould TR, et al. Distinct Ultrafine Particle Profiles Associated with Aircraft and Roadway Traffic. *Environ Sci Technol*. 2021;55(5):2847-2858. doi:10.1021/acs.est.0c05933

70. Hsu, H.-H.; Adamkiewicz, G.; Houseman, E. A.; Zarubiak, D.; Spengler, J. D.; Levy, J. I. Contributions of aircraft arrivals and departures to ultrafine particle counts near Los Angeles

International Airport. Sci. Total Environ. 2013, 444, 347−355.

71. Hudda, N.; Gould, T.; Hartin, K.; Larson, T. V.; Fruin, S. A. Emissions from an international airport increase particle number concentrations 4-fold at 10 km downwind. Environ. Sci. Technol. 2014, 48, 6628−6635.

72. Hudda, N.; Fruin, S. A. International airport impacts to air quality: size and related properties of large increases in ultrafine particle number concentrations. Environ. Sci. Technol. 2016, 50, 3362−3370.

73. Riley, E. A.; Gould, T.; Hartin, K.; Fruin, S. A.; Simpson, C. D.; Yost, M. G.; Larson, T. Ultrafine particle size as a tracer for aircraft turbine emissions. Atmos. Environ. 2016, 139, 20−29.

74. Hudda, N.; Simon, M. C.; Zamore, W.; Brugge, D.; Durant, J. L. Aviation emissions impact ambient ultrafine particle concentrations in the greater Boston area. Environ. Sci. Technol. 2016, 50, 8514− 8521.

75. Hudda, N.; Simon, M. C.; Zamore, W.; Durant, J. L. AviationRelated impacts on ultrafine particle number concentrations outside and inside residences near an airport. Environ. Sci. Technol. 2018, 52, 1765−1772.

76. Masiol, M.; Hopke, P. K.; Felton, H. D.; Frank, B. P.; Rattigan, O. V.; Wurth, M. J.; LaDuke, G. H. Analysis of major air pollutants and submicron particles in New York City and Long Island. Atmos. Environ. 2017, 148, 203−214.

77. US EPA O. Support Center for Regulatory Atmospheric Modeling (SCRAM). Published July 13, 2016. Accessed February 9, 2023. https://www.epa.gov/scram

78. Information by Location | Washington Tracking Network (WTN). Accessed April 21, 2023. https://fortress.wa.gov/doh/wtnibl/WTNIBL/

79. King County Census Tracts. Institute for Health Metrics and Evaluation. Accessed May 22, 2023. https://vizhub.healthdata.org/subnational/usa/wa/king-county

80. Nelson PT, Kukull WA, Frosch MP. Thinking Outside the Box: Alzheimer-Type Neuropathology That Does Not Map Directly Onto Current Consensus Recommendations. *Journal of Neuropathology & Experimental Neurology*. 2010;69(5):449-454. doi:10.1097/NEN.0b013e3181d8db07

81. Revisions to the Guideline on Air Quality Models: Enhancements to the AERMOD Dispersion Modeling System and Incorporation of Approaches To Address Ozone and Fine Particulate Matter. Federal Register. Published January 17, 2017. Accessed May 30, 2023. https://www.federalregister.gov/documents/2017/01/17/2016-31747/revisions-to-the-guideline-on-air-quality-models-enhancements-to-the-aermod-dispersion-modeling

82. R Core Team (2021). R: A language and environment for statistical computing. R Foundation for Statistical Computing, Vienna, Austria. https://www.R-project.org/

83. Lakeview AERMOD. Accessed June 4, 2023. https://www.weblakes.com/software/air-dispersion/aermod-view/